Accotto Cristina (Orcid ID: 0000-0003-4301-6216)
Talavera Cristina (Orcid ID: 0000-0002-4429-7905)
Evans Noreen J. (Orcid ID: 0000-0002-7615-8328)

Tectonic evolution of the Eastern Moroccan Meseta: from Late Devonian fore-arc sedimentation to Early Carboniferous collision of an Avalonian promontory

C. Accotto[1], D. Martínez Poyatos[1], A. Azor[1], A. Jabaloy-Sánchez[1], C. Talavera[2, 3], N. J. Evans[3], and A. Azdimousa[4]

[1] Departamento de Geodinámica, Universidad de Granada, Granada, Spain.

[2] School of Geosciences, University of Edinburgh, Edinburgh, UK.

[3] School of Earth and Planetary Science/John de Laeter Centre, Curtin University, Bentley, Australia.

[4] Faculté Pluridisciplinaire de Nador et Laboratoire des Géosciences Appliquées, Faculté des Sciences, Université Mohammed I, Oujda, Morocco.

Corresponding author: Cristina Accotto (accotto@ugr.es)

Key Points:

- The Debdou-Mekkam Metasediments deposited during the Late Devonian (Early Tournaisian?) closure of the Rheic Ocean on the N-Gondwanan margin
- An important input of Mesoproterozoic and Devonian detrital zircons points to Avalonian basement and arc sources
- The collision between an Avalonian promontory and N-Gondwana deformed the Debdou-Mekkam metasediments forming a SE-vergent fold belt

This article has been accepted for publication and undergone full peer review but has not been through the copyediting, typesetting, pagination and proofreading process which may lead to differences between this version and the Version of Record. Please cite this article as doi: 10.1029/2019TC005976

Abstract

The deformed Paleozoic succession of the Eastern Moroccan Meseta crops out in relatively small and isolated inliers surrounded by Mesozoic and Cenozoic rocks. Two of the largest inliers (Mekkam and Debdou) are characterized by a monotonous succession of slates and greywackes affected by polyphasic folding that occurred at low- to very low-grade metamorphic conditions. New U-Pb ages on detrital zircon grains from the Debdou-Mekkam Metasediments constrain the maximal depositional age as Late Devonian, interpreted to be close to the true sedimentation age. Furthermore, the ε_{Hf} values of the Devonian detrital zircons, together with the presence of a series of scattered zircon grains with ages between c. 0.9 and c. 1.9 Ga suggest provenance from a subduction related magmatic arc located on the Avalonian margin.

The Debdou-Mekkam massif is characterized by an Early Carboniferous first deformational event (D1), which gave way to a pervasive cleavage (S1) associated with plurikilometric-scale, tight to isoclinal, overturned to recumbent folds. Later events (Dc) occurred at Late Carboniferous time and generated variably developed crenulation cleavages (Sc) associated with variously oriented metric- to kilometric-scale folds, which complicate the pattern of both D1 intersection lineations (L1) and axial traces. The restoration of this pronounced curved pattern yields originally SW-NE oriented D1 fold axes with regional SE-vergence. This important Early Carboniferous shortening and SE-directed tectonic transport can be explained by closure of the Rheic Ocean and the first phases of the collision between the northern passive margin of Gondwana and an Avalonian promontory.

1 Introduction

The recognition of ophiolites in old collisional orogenic belts is the most valuable evidence of ancient oceanic closure and continental docking (e.g., Dewey & Bird, 1971). However, the complete consumption of oceanic lithosphere is common in subduction zones, which makes many orogenic sutures appear as cryptic (e.g., Pérez-Cáceres et al., 2015; Schulmann et al., 2014). In these cases, indirect lines of evidence (e.g. recognition of paleogeographically exotic terranes and presence of high-pressure and/or intensely deformed belts) are usually employed to locate orogenic sutures and account for plate tectonic reconstructions (e.g., Franke et al., 2017; Matte, 2001; Romer & Kroner, 2019; Van Hinsbergen et al., 2019).

The Late Paleozoic Variscan/Alleghanian Belt (Figure 1a) is frequently discussed in terms of the meaning and correlation of the orogenic sutures along the different transects (e.g. Díez Fernández & Arenas, 2015; Faryad & Kachlik, 2013; Martínez Catalán et al., 2019; Pérez-Cáceres et al., 2015). The Variscan orogeny resulted from Rheic Ocean consumption and subsequent collision between Gondwana and Laurussia, with the final assembly of the Pangea supercontinent by the end of the Paleozoic (e.g. Matte, 2001). Before that, Early Paleozoic rifting along the northern Gondwana margin gave way to the opening of the Rheic Ocean during the drifting of continental domains (collectively called Avalonia) that were connected to the western part of northern Gondwana (Amazonia; Murphy et al., 2006) at Neoproterozoic time. On the other hand, Laurussia resulted from the amalgamation of Laurentia, Baltica and Avalonia during mid-Paleozoic time (Caledonian Orogeny s.l.).

Only a few of the sutures-related units recognized along the Variscan Belt preserve ophiolites, which were classically considered the remnants of the Rheic Ocean (e.g. Matte, 2001) and were later reinterpreted as witnessing minor younger oceanic realms (e.g. Arenas

et al., 2014; Martínez Catalán et al., 2019; Shail & Leveridge, 2009). Thus, no direct relicts of the Rheic Ocean seem to crop out along the Variscides, which compromises all of the available paleogeographic reconstructions. Actually, the Rheic Ocean has been located based on indirect data derived from paleomagnetic, geochemical, and geochronological studies (e.g. Gärtner et al., 2013; Villeneuve et al., 2015, in the SW Moroccan transect; Hoepffner et al., 2005; Michard et al., 2010; Simancas et al., 2005; Tahiri et al., 2010, in the NW Moroccan transect; Azor et al., 2008; Braid et al., 2011; Pérez-Cáceres et al., 2017, 2015, in the SW Iberian transect; Arenas et al., 2014; Martínez Catalán et al., 2019, in the NW Iberian transect; and Franke et al., 2017, in the central European transect).

The present-day dispersed configuration of the Variscan/Alleghanian Orogeny is the result of large-scale Late Carboniferous-Early Permian right-lateral wrenching, Pangea breakup and Alpine reworking. The Gondwanan side of the Variscan Belt crops out in a number of massifs distributed from western and central Europe to NW Africa (Figure 1a). In northern Morocco (Figure 1b), erosion of the Triassic-Cenozoic cover has exposed several deformed Paleozoic massifs (collectively known as the "Moroccan Variscides") in the Moroccan Meseta and High Atlas; southwards, the front of the Variscan Belt can be traced through the almost undeformed Paleozoic series of the Anti-Atlas region. Previous regional tectonic studies (El Hassani et al., 2003; Hoepffner, 1987; Hoepffner et al., 2005, 2006; Michard et al., 2008, 2010; Piqué, 1994, 2001; Piqué & Michard, 1981, 1989; Simancas et al., 2005, 2009; Tahiri & Hoepffner, 1988) subdivided the Moroccan Variscides into different domains (Coastal Block, Western Moroccan Meseta, Eastern Moroccan Meseta, and High Atlas or Sub-Meseta Domain; Figure 1b) based on stratigraphic and tectonic differences that would have paleogeographic implications (Michard et al., 2010 and references therein). The boundaries between these domains are regional-scale fault zones that reactivated former narrow rifted areas (Hoepffner et al., 2005, 2006; Michard et al., 2010). Nevertheless, the paleogeographic relevance of these structures is unclear, since they do not include suture-related rocks (e.g. ophiolites), and the Ordovician-Devonian stratigraphic successions in all the Moroccan Variscides, as well as in other zones of the northern margin of Gondwana, indicate deposition in a shared passive margin (Piqué, 1994; Simancas et al., 2009), suggesting that all the domains of the Moroccan Variscides remained attached to northern Gondwana throughout the Paleozoic. This paleogeographic affinity is also supported by the detrital zircon provenance studies performed to date (Abati et al., 2010; Accotto et al., 2019; Avigad et al., 2012; El Houicha et al., 2018; Ghienne et al., 2018; Letsch et al., 2018), which suggest a Gondwanan provenance for the Cambrian to Devonian sediments of the Moroccan Variscides. The only exception would be the Sehoul Block in the Western Moroccan Meseta (Figure 1b), which is thought to have an Avalonian derivation based on the presence of a mid-Paleozoic (i.e. Caledonian) deformation occurred before the emplacement of granites radiometrically dated at the Late Devonian (U-Pb on zircons; Tahiri et al., 2010).

This work aims to unravel the Late Paleozoic tectonic evolution of the complex and poorly known Debdou-Mekkam Massif in the Eastern Moroccan Meseta (Figure 1b). To do so, a detailed structural study of the metasedimentary Paleozoic rocks of this area was carried out, together with U-Pb geochronology and Hf isotope systematics on detrital zircon grains. This approach helped to constrain rock ages, provenance and tectonic evolution in the context of the Moroccan Variscides. On a broad scale, a new tectonic model emerges which highlights the close influence of the Rheic Ocean suture in the Eastern Moroccan Meseta, although the suture itself seems to be concealed and, hence, cryptic, as well as in many other transects of the Variscan Belt.

2 Geological setting

Paleozoic rocks are exposed in the Eastern Moroccan Meseta in relatively small (from a few square kilometers up to c. 1200 km^2) and isolated inliers (Figure 1b), characterized by Cambrian-Permian successions deformed by Eovariscan (Late Devonian-Early Carboniferous) to Variscan (Carboniferous) events (Hoepffner, 1987). The Ediacaran basement that crops out in several areas of the Western Moroccan Meseta and Coastal Block (e.g. El Haibi et al., 2020; El Houicha et al., 2018; Ouabid et al., 2017; Pereira et al., 2014, 2015; Tahiri et al., 2010) has not been reported in the Eastern Moroccan Meseta. Thus, the oldest sedimentary rocks described in this latter region are shales and schists attributed to the Cambrian-Ordovician in the Midelt Massif by correlation with similar facies in the Western Moroccan Meseta (Hoepffner, 1989). Only the highest levels of this succession were dated in Tazekka based on their paleontological and palynological content, which yielded Early Ordovician ages (Desteucq & Fournier-Vinas, 1981; Hoepffner, 1977; Rauscher et al., 1984). The overlying quartzitic sandstones, attributed to the Late Ordovician, reach maximum thickness at Tazekka (Hoepffner, 1989). The Silurian succession is characterized by black fine-grained quartzitic sandstones and shales with graptolites. Based on palynological content, the Devonian consists of slates followed by siliciclastic flysch sediments dated at Emsian (Marhoumi et al., 1983).

The Devonian flysch marks the change from a passive margin context, more or less continuous since the Cambrian, to a subsiding basin that preceded an "Eovariscan" tectonic event associated with the partial exhumation of the Moroccan Meseta (Hoepffner, 1987, 1989). In the Eastern Moroccan Meseta, the different inliers were variably affected by this "Eovariscan" deformation, which associated with very low-grade metamorphism, although greenschist to amphibolite facies conditions were locally reached (Midelt and North Tamlet areas); the available ages point to the Late Devonian for the "Eovariscan" event: 366 ± 7 Ma obtained with Rb-Sr methods in the Midelt area (Clauer et al., 1980; Tisserant, 1977); 372.3 ± 8.1 and 368.3 ± 7.9 Ma obtained with the K-Ar method on syn-deformational illite grains from the Debdou and Mekkam Massifs, respectively (Huon et al., 1987). Hoepffner (1987) proposed that the "Eovariscan" tectonic event comprises two stages in the Midelt and Tamlet regions, both characterized by NW-SE trending isoclinal recumbent or overturned folds with W- to SW-vergences. The first of these stages would be associated with the development of a slaty cleavage, while the second would be related to a crenulation cleavage, horizontal shear and stretching lineation (Hoepffner, 1987; Hoepffner et al., 2006).

An "Intravisean" extensional phase (Hoepffner et al., 2006), associated with a transgression and the opening of volcano-clastic basins in the northern part of the Eastern Moroccan Meseta, was also described (e.g. Debdou-Mekkam, Jerada, Traras basins, Figure 1b). The Late Visean sedimentary rocks were dated based on their fossil fauna content (Médioni, 1979 and references therein); they locally contain (e.g. in the Mekkam region) a basal level of limestones and carbonatic breccias, which unconformably overlie the Cambrian-Devonian succession. The Late Visean volcanosedimentary deposition was accompanied by the emplacement of granitoids (El Hadi et al., 2006 and references therein).

The main Variscan event was described as responsible for E-W to ENE-WSW oriented, N-vergent folds (Hoepffner et al., 2006) that occurred at very low-grade metamorphic conditions during Late Carboniferous (c. 300 Ma; K-Ar methods on neoformed micas from the Tazekka Massif; Huon et al., 1987). This event was followed by the emplacement of several post-kinematic granitoids (c. 290 Ma; El Hadi et al., 2003, 2006 and references therein). Finally, Late Carboniferous-Early Permian tardi-Variscan events affected

the Eastern Moroccan Meseta giving way to mainly compressional E-W, NW-SE, and N-S faults (Hoepffner et al., 2006).

The Permian post-orogenic continental red-beds that characterize the Western Moroccan Meseta and the Coastal Block (Hoepffner et al., 2005) have not been described in the Eastern Moroccan Meseta, where Lower Triassic red shales and basalts directly overlay in unconformity over the Carboniferous (Visean-Westphalian) volcano-sedimentary rocks.

2.1 The Debdou-Mekkam massifs

The Debdou-Mekkam massifs (comprising the Paleozoic outcrops in the Debdou and Mekkam areas, and a few smaller inliers between them; Figure 2) are characterized by a monotonous sequence of siliciclastic turbidites, previously called "Mekkam schists" (Hoepffner, 1987 and references therein). We prefer to refer to them as the "Debdou-Mekkam metasediments" (DMMS), because of the low-grade metamorphic imprint that these rocks underwent (as compared with the non-metamorphic overlying succession). The DMMS were originally dated as Tournaisian-Late Visean by Médioni (1980), based on the presence of fragments of fossil plants. However, palynological data (Marhoumi, 1984; Marhoumi et al., 1983) yielded Middle-Late Devonian ages (Givetian-Frasnian).

From a lithological point of view, the DMMS are an irregular alternation of slates and greywackes. The slates are particularly predominant in the minor inliers and, locally, in the Debdou and Mekkam areas; they are composed by very fine-grained sediments with abundant detrital mica (Figure 3a). The coarse-grained portion of the sequence is characterized by decimetric- to decametric-thick beds of greywackes with subordinate sandstones, quartzitic sandstones, arkoses, and, locally, microconglomerates (Figure 3b); under the microscope, these rocks show abundant quartz (often rounded), fragments of magmatic crystalline rocks, phyllosilicates (mica and clay), and oxides. The DMMS often show sedimentary structures, such as ripple laminations (Figure 3c) or graded bedding (Figure 3d), which were used in the field to identify the polarity of the sequence. The basal contact of the DMMS is not exposed in the region, hence its global thickness is unknown. The metamorphism is of very low- to low-grade with the phyllosilicate-rich rocks occurring as slates to phyllites.

The DMMS are unconformably overlain by a Visean succession, characterized by a basal breccia with carbonate cement and clasts of quartzitic sandstones and slates, probably reworked from the underlain sequence, and fragments of volcanites (Figure 3e), followed by limestones containing fragments of brachiopods and polyps of Late Visean age (Médioni, 1979 and references therein). The succession continues upwards with a 300 m-thick series of tuffs with interbedded rhyolites, trachyandesites and radiolarites, followed by a thick series of slates and sandstones, paleontologically dated at Late Visean (Médioni, 1979 and references therein). The Visean unconformity (Figure 3f) crops out in the southern zone of Mekkam area, NW of Hassiane Ed Diab (Figure 3), where is partially affected by a WNW-ESE trending fault (Section 4.4).

3 Detrital zircon geochronology

3.1 U-Pb analyses

Four to five kilograms of rock were collected from five outcrops of the DMMS (Figure 2). DEB2 (IGSN: IEACC0005) is a greywacke sampled in the Debdou inlier and

made up of abundant fine-sized (c. 0.1 mm in diameter) quartz and phyllosilicate grains, with subordinate altered feldspars and oxides. MIM2 (IGSN: IEACC0004) is a quartzitic sandstone sampled in the westernmost Lalla Mimouna-Oued Awam inliers, and composed of dominant medium-sized (c. 0.2 mm in diameter) quartz grains with subordinate phyllosilicates and oxides, which define the main cleavage. Samples OUJ10 (IGSN: IEACC0001), OUJ11 (IGSN: IEACC0002), and OUJ13 (IGSN: IEACC0003) were collected in the Mekkam inlier. OUJ10 is an arkose characterized by medium-sized (c. 0.2 mm in diameter) quartz grains, slightly oriented parallel to the main cleavage, which is defined by phyllosilicates. OUJ11 was sampled not far from OUJ10 (but in a different outcrop) and is a coarse-grained (c. 0.25-0.3 mm in diameter) arkose with abundant quartz and mica clasts; this latter is partially recrystallized, which suggests a slight metamorphic overprint. Finally, OUJ13 is a quartz-rich sandstone with abundant phyllosilicate grains and the quartzitic clasts varying from fine to medium in size (diameter from c. 0.1 mm to c. 0.2 mm).

All the samples were processed in the laboratories of the University of Granada (Spain). They were crashed, and detrital zircon grains were separated using granulometric (sieves) and density (panning) separation procedures. Finally, 150-250 zircon grains were handpicked from each sample and sent to the John de Laeter Centre (JdLC) at Curtin University in Perth (Australia), where they were imaged by cathodoluminescence using a Mira3 FESEM instrument at the Microscopy and Microanalysis Facility (a selection of cathodoluminescence images of the most representative grains is included in the Supporting Information, Figures S1 to S5), and then analyzed with Laser Ablation Inductively Coupled Plasma Mass Spectrometry (LA-ICPMS). In order to have a statistically significant amount of data (Vermeesch, 2004), a minimum of 146 analyses were carried out on each sample and the results that showed a discordance higher than 10% were considered anomalous and not accounted further. Given the increased errors associated with $^{206}Pb/^{238}U$ values observed for ages older than 1500 Ma, this ratio was only used to date younger grains; for ages older than 1500 Ma, the $^{207}Pb/^{206}Pb$ ratio was considered more appropriate. The detailed analytical methodology is provided in the Supporting Information (Text S1). The statistical analysis of the data was carried out using DensityPlotter 8.4 software (Vermeesch, 2012). The histograms were created using a bin of 40 Ma, while an adaptive bandwidth of 40 Ma was applied for the Kernel Density Estimators (KDE). The youngest detrital zircon populations were calculated with IsoplotR online (Vermeesch, 2018). Errors are expressed at the 1σ level. The raw analytical results are listed in Table S1 of the Supporting Information.

3.1.1 Results

The zircon grains separated from the studied samples are between 100 μm and 300 μm in length. Most of the grains are yellowish or whitish; some of them are rounded, while others are euhedral; a few zircons are purple to pink, with a generally rounded shape. Cathodoluminescence images (Figures S1 to S5 in the Supporting Information) show continuous oscillatory zoning, partially reabsorbed cores with low or high U overgrowth rims, sector zoning, or structureless grains.

From sample DEB2 (Figure 4a), 150 analyses were carried out on 147 detrital zircon grains, yielding 139 concordant results. Fifty-nine percent of the data (n = 82) range from c. 690 to c. 540 Ma and represent a main population with an Ediacaran mean age of 605.1 ± 0.4 Ma. Two minor detrital zircon populations yielded Paleoproterozoic mean ages, with two peaks at 2071.1 ± 2.7 Ma (c. 1.96-2.29 Ga, 16.5%) and 2458.8 ± 4.5 Ma (c. 2.49-2.43 Ga, 6.5%). A number of scattered data gave Cambrian (n = 4, c. 532-503 Ma), Tonian-Ectasian (n = 11, c. 1346-823 Ma), Orosirian (n = 5, c. 1938-1771 Ma), and Archean (n = 3, c. 3.0-2.7 Ga) ages. The youngest detrital zircon population in this sample (n = 9) yielded a Late

Ediacaran weighted average age (549.6 ± 1.2 Ma, MSWD = 1.12); however, the 2 youngest detrital zircon grains gave Late Devonian (Late Frasnian) ages (374-375 Ma).

One hundred thirty-five detrital zircon grains from sample MIM2 were analyzed (Figure 4b) and 146 analyses were carried out, with 130 yielding concordant results. The main detrital zircon population has an Ediacaran mean age (616.3 ± 0.4 Ma; c. 786-547 Ma) and comprises the 50.8% of the data (n = 66). Furthermore, three minor populations can be defined: a Late Devonian population (average age of 369.6 ± 0.6 Ma; c. 380-357 Ma) that comprises 6.2% of the concordant data (n = 8), a c. 2013-2221 Ma Paleoproterozoic peak (2095.2 ± 3.8 Ma, 13.8%, n = 18), and a c. 2.43-2.6 Ga Siderian-Neoarchean population (mean age 2493.9 ± 4.2 Ma, 10%, n = 13). Scattered data gave Cambrian (n = 2, c. 523-501 Ma), Tonian-Orosirian (n = 14, c. 1940-873 Ma), and Mesoarchean (n = 9, c. 2.7-3.1 Ga) ages. The youngest detrital zircon population is Late Devonian (weighted average age 370.4 ± 0.9 Ma, MSWD = 1.28) and includes 4 data.

One hundred ninety detrital zircon grains from sample OUJ10 were analyzed (Figure 4c) and 200 analyses were carried out, yielding 180 concordant results. The two main detrital zircon populations yielded mean ages of 615.9 ± 0.9 Ma (Ediacaran; c. 790-541 Ma, 39.4%, n = 71) and 371.4 ± 0.8 Ma (Late Devonian; c. 425-320 Ma, 19.4%, n = 35). Nine percent of the data (n = 16) are included in a minor Tonian-Stenian population (mean age of 1073.6 ± 2.9 Ma; c. 1215-847 Ma) and 12.2% in a Paleoproterozoic peak (mean age of 2078.1 ± 3.3 Ma; c. 2.23-1.94 Ga). Scattered data yielded Cambrian (n = 7, c. 538-514 Ma), Ectasian-Orosirian (n = 19, c. 1.28-1.9 Ga), and Siderian-Archean (n = 10, c. 2.44-2.83 Ga) ages. The youngest detrital zircon population in this sample is Late Devonian (weighted average age 361.7 ± 1.7 Ma, MSWD = 1.25) and includes 7 data.

From sample OUJ11 (Figure 4d), 301 analyses were performed on 269 zircon grains, yielding 267 concordant results. The main detrital zircon populations yielded Ediacaran (mean age of 627.4 ± 0.8 Ma; c. 823-543 Ma, 39.3%) and Late Devonian (mean age of 376.9 ± 0.6 Ma; c. 426-343 Ma, 23.2%, n = 62) ages. Seventeen percent of the data (n = 45) can be grouped into a minor Paleoproterozoic population with a mean age of 2089 ± 2.5 Ma (c. 2.35-1.99 Ga). Scattered data yielded Cambrian (n = 9, c. 538-499 Ma), Tonian-Orosirian (n = 35, c. 1931-975 Ma), and Archean (n = 11, c. 3.37-2.47 Ga) ages. The youngest detrital zircon population is composed of 9 data with a Late Devonian weighted average age (362.3 ± 1.3 Ma, MSWD = 1.02).

Finally, from sample OUJ13 (Figure 4e), 149 grains were analyzed yielding 150 results, 146 of which were concordant. Thirty-seven percent of the data (n = 35) are included in a main detrital zircon population with Late Devonian mean age (peak at 378 ± 0.3 Ma), with individual ages ranging from c. 417 Ma to c. 296 Ma. Another main population yielded a Cryogenian mean age of 649.3 ± 0.5 Ma (c. 811-543 Ma, 31.5%, n = 44). Fourteen percent of the data (n = 21) are included in a minor Paleoproterozoic peak with a mean age of 2079.2 ± 2.9 Ma and an age range of c. 2.23-1.93 Ga. Scattered analyses gave Cambrian (n = 2, c. 494-510 Ma), Tonian-Orosirian (n = 22, c. 1840-898 Ma), and Archean (c. 3.5-2.6 Ga, n = 3) ages. The youngest detrital zircon population (n = 4) yielded a Late Devonian age (weighted average age 360 ± 1.1 Ma, MSWD = 1.16).

In summary (Figure 4f and g), all samples are characterized by an important Ediacaran-Cryogenian detrital zircon population (peaked at c. 618 Ma and comprising c. 30-60% of the data) and by minor Paleoproterozoic-Archean populations (c. 2.1 Ga, c. 15%, and c. 2.5 Ga, c. 4%). Finally, a Devonian detrital zircon population (c. 375 Ma) can be dominant (OUJ10, OUJ11, and OUJ13; 20-35%), secondary (MIM2, 6%), or almost absent (DEB2),

thus pointing to a Late Devonian maximum depositional age for the DMMS. Scattered data with Tonian-Orosirian ages are common in all the samples (as highlighted in Figure 4h).

3.2 Hf isotope analyses

The four samples characterized by the Devonian detrital zircon population were analyzed for Hf isotopes with the aim of defining their isotopic signature. Therefore, Hf isotopes were not analyzed on sample DEB2, where only two Devonian zircons were found.

Hf isotopes in zircon were measured at the Geohistory facility in the JdLC, Curtin University (Australia). Previously dated zircon crystals were ablated using a Resonetics resolution M-50A excimer laser, coupled to a Nu Plasma II multi-collector inductively coupled plasma mass spectrometer (LA-MC-ICPMS). All isotopes (^{180}Hf, ^{179}Hf, ^{178}Hf, ^{177}Hf, ^{176}Hf, ^{175}Lu, ^{174}Hf, ^{173}Yb, ^{172}Yb, and ^{171}Yb) were counted on the Faraday collector array. Calculation of ε_{Hf} values employed the decay constant of Scherer et al. (2001) and the Chondritic Uniform Reservoir (CHUR) values of Blichert-Toft & Albarède (1997). The detailed analytical methodology and results are included in the Supporting Information, Text S2 and Table S2 respectively.

To calculate Hf model ages of the continental crust (T_{NC}) where the Devonian zircon grains were formed, the new continental crust composition of Dhuime et al. (2011) was used, which is more isotopically enriched than the depleted mantle and similar to the composition of island arc rocks.

3.2.1 Results

One hundred and twenty-nine analyses were carried out on detrital zircon grains from sample MIM2 (Figure 5a). The Devonian zircon population (mean age of 369.6 ± 0.6 Ma) is characterized by slightly negative (-6 to 0; n = 8) ε_{Hf} values and T_{NC} between 1.2 Ga and 1.6 Ga. The Ediacaran detrital zircon population (mean age of 616.3 ± 0.4 Ma) is characterized by a very wide range of ε_{Hf} values (from -24 to +12, n = 68), as is the Paleoproterozoic population (mean age of 2095.2 ± 3.8 Ma, ε_{Hf} values from -13 to +6, plus an isolated value at +15, n = 18). The Siderian-Neoarchean peak (2493.3 ± 4.2 Ma) shows mostly negative ε_{Hf} (from -10 to +3, n = 12). The scattered Tonian-Orosirian grains mainly yielded positive ε_{Hf} values (from -10 to +11, n = 14), while the scattered Archean grains mostly displayed negative values (-17 to +2, n = 9).

On the detrital zircons from sample OUJ10, 59 Hf isotope analyses were performed (Figure 5b). Ten grains from the Devonian population (mean age of 371.4 ± 0.8 Ma) were analyzed: nine yielded positive ε_{Hf} values from +0 to +6, while one gave a ε_{Hf} value of -4; T_{NC} varies between 0.7 Ga and 1.5 Ga. The Ediacaran peak (607.4 ± 0.8 Ma, n = 27) yielded a wide range of ε_{Hf} values ranging from -21 to +10, while the Paleoproterozoic peak (2078.1 ± 3.3 Ma, n = 7) is characterized by mostly positive values (-1 to +5), with an isolated strongly negative result (-17). The scattered Tonian-Orosirian zircons yielded mostly positive ε_{Hf} values (-2 to +3), with a couple of strongly negative data (-20 and -17). Two Archean grains gave negative values (-7 and -4).

One hundred and twenty-eight analyses were performed on detrital zircons from sample OUJ11 (Figure 5c). Twenty-one Devonian zircons (peak at 376.9 ± 0.6 Ma) yielded mainly positive ε_{Hf} values varying from -0.4 to +6 and T_{NC} varying from 0.6 Ga to 1.3 Ga. The ε_{Hf} range increases for the Ediacaran peak (627.4 ± 0.8 Ma, n = 56, ε_{Hf} from -24 to +12) and the Paleoproterozoic peak (2089 ± 2.5 Ma, n = 27, ε_{Hf} from -2 to +9). The scattered

Tonian-Orosirian zircons yielded variable values (from -20 to +7) with predominance of positive values, while the Archean zircons yielded negative values between -13 and -3.

Finally, 125 analyses were carried out on grains from sample OUJ13 (Figure 5d). The Devonian detrital zircon population (mean age 378 ± 0.3 Ma) is characterized by mostly positive ε_{Hf} values ranging from -1 to +8 (n = 47) and T_{NC} between 0.8 Ga and 1.2 Ga. The Ediacaran peak (649.3 ± 0.5 Ma, n = 39) yielded a very wide range of values (-25 to +12) and the Paleoproterozoic peak (2079.2 ± 2.9 Ma, n = 17) mostly gave positive values (-6 to +6), with an isolated strongly negative ε_{Hf} value (-15). Twenty scattered Tonian-Orosirian zircons yielded a wide range of values (-16 to +13). Two Archean data gave ε_{Hf} values of -3 and +3.

In summary (Figure 5e), the Devonian detrital zircon population is characterized by mostly (> 80% of the data) positive ε_{Hf} values ranging from -6 to +8, except for those in sample MIM2 which gave slightly negative values (between 0 and -6). The T_{NC} vary from 0.6 Ga to 1.6 Ga. The Ediacaran and Paleoproterozoic populations are characterized by a very wide range of ε_{Hf} values (-25 to +12, and -17 to +9, respectively). The scattered Tonian-Orosirian grains yielded mostly positive ε_{Hf} values, while the Siderian-Archean zircons gave mostly negative values.

4 Structural analysis

From a structural point of view, the Debdou-Mekkam Massif was previously described by Hoepffner (1987), who identified two “Eovariscan” deformational events. According to this author, the main deformation produced W-vergent structures related to an important shortening, though neither detailed structural maps, nor cross-sections of the inliers were provided.

Based on our field observations, the Debdou-Mekkam Massif is characterized by a polyphasic deformation. The first event (D1) is characterized by a pervasive cleavage (S1) associated with plurikilometric-scale SE-vergent folds. Later event (or events; Dc) generated variably developed crenulation cleavages (Sc) associated with differently oriented metric- to kilometric-scale folds. All of the cleavages observed are aligned with the axial-plane to the respective folding phase. Neither mineral/stretching lineations, nor structures indicative of simple shear deformation were observed. Some post-Variscan (post Dc) rectilinear fractures can locally limit the Paleozoic inliers (Figure 2). Our structural analysis focused on the D1 structures at outcrop scale and large-scale reconstruction.

4.1 Main tectonic fabrics

4.1.1 Early fabric

The earliest tectonic fabric recognizable is a foliation (S1) superimposed on the stratigraphic bedding (S0; Figure 3). Since overturned folds are present, a careful inspection of sedimentary polarity criteria was carried out, e.g. graded bedding, basal erosive surfaces, geometry of sedimentary sets with cross lamination, and recognition of Bouma sequences (Figure 3c and d). S1 is a slaty (locally disjunctive) cleavage, well developed in phyllosilicate-rich beds, and less penetrative in coarse-grained layers, where refraction with respect to S0 is more intense (Figure 6). The obliquity between S0 and S1 usually defines a well-developed intersection lineation (L1). S1 represents the axial-planar cleavage of milimetric- to decametric-scale folds (Figure 6a, b, and e) and the orientation of L1 roughly

indicates the hinge orientation. The folds are tight to isoclinal, inclined to recumbent, and often asymmetric. Fold asymmetry (S or Z shapes), together with local vergence (i.e. S0-S1 relationships; Bell, 1981) (Figure 6c, d and f) and stratigraphic polarities (Figure 3c and d) were systematically examined in order to reconstruct the large-scale D1 structure in the Debdou-Mekkam Massif. When D1 folds are not affected by later deformations, normal limbs are low-dipping and S1 is not very penetrative; on the contrary, overturned limbs show higher dips and more penetrative S1.

At microscopic scale, S1 is easily visible and defined by the sharp and continuous orientation of white mica, chlorite, and Fe-oxides (Figure 6e and f). In coarse-grained layers, S1 is a rough to anastomosing spaced cleavage, marked by the orientation of Fe-oxide concentrates, but less penetrative than within the fine-grained pelitic domains. When S1 presents an anastomosing geometry, it isolates sigmoidal-shaped quartz- and feldspar-rich domains.

4.1.2 Late fabrics

The late ductile deformational event (or events; Dc) generated folds with axial-planar cleavages (Sc) that refold and crenulate the previous structures (Figure 7a and e). The visible folds are, centimetric- to metric-scale (Figure 7b), open to tight, and they feature chevron or kink-band geometries. The orientation of the folds (and their corresponding axial-planar crenulation cleavages) is variable, and they can be grouped into three sets: two of them have steeply dipping to vertical axial planes trending NW-SE (Sc1) and NE-SW (Sc2) respectively; the third set (Sc3) is associated with low-dip to horizontal axial-plane kink-folds.

At the outcrop scale, the penetrative nature of Sc varies from absent (only S0+S1 is observed), to spaced crenulation cleavage, to centimetric- to decimetric-scale tectonic banding (Figure 7c and d). The distribution of Dc folds and related crenulation cleavages is heterogeneous across the Debdou-Mekkam Massif, and they rarely appear superposed at the outcrop scale, making the geometric and temporal relationships among the three sets unclear. Therefore, the interpretation of their genesis remains ambiguous: (i) they might be the result of successive deformational phases occurred under different regional stress orientations, or (ii) a unique deformational event resulted in different crenulation orientations due to local interference with the pre-existing, variably oriented, D1 structures (see section 5.3). Whatever the case, we have taken into account the geometry of the crenulation folds during the reconstruction of the D1 structures (the main purpose of our structural analysis), while the proposed tectonic evolution is restricted to the D1 event in order to avoid possible misinterpretations derived from the uncertain meaning of Dc structures.

At microscopic scale, Sc only appears in the phyllosilicate-rich layers as a spaced cleavage with anastomosing geometry defined by Fe-oxides (Figure 7e). Sometimes, Sc also deforms the previous S1 and S0 forming micro-kink bands (Figure 7f).

4.2 The Debdou inlier

The Debdou inlier has been divided into two sectors according to the orientation of S1 and L1. The southern sector (Figure 8) is characterized by variable trends of S1 (from NW-SE, through N-S, to NE-SW), with dominant low dips to the west and L1 mostly plunging to the south. In the R'chida area (western portion of cross-section A-A', Figure 8), a normal limb crops out, characterized by sub-horizontal S0 with a few indicators of normal polarity, and S1 gently dipping to the NW with L1 gently plunging to the SW. The local vergence of

D1 is to the SE. A vertical E-W trending crenulation cleavage (Sc1) is present, though scarcely penetrative. In the eastern portion of cross-section A-A' (Figure 8), S1 and L1 trends rotate to NW-SE and a D1 hinge zone is observed. Similar L1 orientations are observed in the Galbi Al Hayyar area (cross-section B-B'; Figure 8), where S1 is sub-horizontal and S0 dips gently to the SW with reverse polarity. The local D1 vergence in this area is to the SW. To the SE, along cross-section B-B', the stratigraphic polarity is normal for a couple of kilometers, with S0 and S1 dipping to the SW, and showing the angular relationships typical of a normal limb. L1 is rotated with respect to the Galbi Al Hayyar area, being now oriented NE-SW and gently plunging to the SW. The asymmetry of the D1 parasitic folds and the relationships between S0 and S1 indicate local SE-vergence. In the remaining eastern portion of cross-section B-B' (Oulad Tayar area), S0 dips moderately to the west and repeated evidence of reverse polarity are observed (mainly graded bedding; Figure 3b). S1 and L1 are NE-SW to N-S trending, the cleavage dips gently to moderately to the west, and L1 plunges to the SSW. S0/S1 relationships and the asymmetry of the mesoscale D1 folds indicate local W-vergence. In one outcrop, a top-to-the-east, low-dipping thrust plane was observed crosscutting the S1 (cross-section B-B', Figure 8), which can be interpreted as a late-D1 brittle structure that contributed to shortening accommodated by D1 folds.

To the SE of Alouana, (Al Kbila area, cross-section C-C'; Figure 8), normal limb relationships dominate with NE-SW trending S0 and S1, and low-dips towards the NW and SE due to Sc2 folds. L1 is NE-SW trending and sub-horizontal. D1 local vergence, defined mostly by the asymmetry of the mesoscale folds, is to the SE. Towards Alouana, the crenulation cleavage Sc2 (NE-SW trending and highly-dipping) intensifies, while contact metamorphism due to the nearby Alouana pluton obliterates the previous structures.

The northern sector of the Debdou inlier (cross-section D-D', Figure 8) is mostly characterized by NW-SE trending, SW-dipping S1, and L1 plunging to the NW. In the Debdou and Bou Ayach areas, S0 shows evidence of reverse polarity (cross-laminations and internal graded bedding). The crenulation cleavage is penetrative, with three different orientations: Sc1, with NW-SE trends and high dips, which is probably responsible for the dip variation of S0 and S1 from SW to NE; Sc2, with NE-SW trends, which is particularly prominent SW of Debdou; and Sc3, which is locally very penetrative east of Debdou and close to Bou Ayach, where Sc3 develops a sub-horizontal tectonic banding (Figure 7c and d). Finally, normal stratigraphic polarities were observed further NE, close to El Sellawit village, where S0 is sub-horizontal, S1 dips gently to the SSW and the local vergence is to the NE. No crenulation cleavages were observed in this area.

4.3 The Lalla-Mimouna-Oued Awam inliers

These inliers extend from Lalla Mimouna to the valley of the Oued Awam, covering a sector in between the two large-scale Paleozoic outcrops of Debdou and Mekkam. In the westernmost inlier, the so called "Inlier 1" in Figure 9 (cross-sections E-E' and F-F'), S0 and S1 have NE-SW to ENE-WSW trends and dip gently to moderately both to the NW and SE as the result of late Dc open upright folds with E-W to ENE-WSW trends. The crenulation cleavage associated with these folds is locally penetrative and often obliterates the S0/S1 relationships. Where the S0/S1 relationships are preserved, they show dominant SE-vergences, although some NW-vergences suggest the presence of local overturned limbs related to parasitic D1 folds developed on a dominant normal limb (cross-sections E-E' and F-F'; Figure 9).

In the central inlier ("Inlier 2" in Figure 9), the trend of the D1 structures is WNW-ESE, with both S0 and S1 gently dipping to the NNE. The bedding polarity is generally normal, though reverse polarity is also found locally (cross-section G-G', Figure 9). Where the polarity is normal, S0/S1 relationships and the asymmetry of small-scale parasitic D1 folds indicate local vergence to the south. A N-S highly dipping crenulation cleavage locally affects the previous structures.

In the eastern inlier ("Inlier 3" in Figure 9), the D1 structures show similar orientation as in "Inlier 1": both S0, S1 and L1 are WSW-ENE trending. As showed in cross-section H-H' (Figure 9), S0 and S1 dip steeply to the NW and SE, due to Dc upright folding. The observed polarity is generally normal and the local vergence of D1 structures is to the SE. In the northern and central sectors of the inlier, the crenulation cleavage trends NE-SW (Sc2), while in the southern one it has NW-SE trends (Sc1).

4.4 The Mekkam inlier

In the Mekkam inlier, the dominant structural grain is NW-SE due to upright Dc folds (Sc1), with the exception of the southwestern and northwestern sectors where the dominant structural orientations are controlled by NE-SW trending Dc folds (Sc2) (Figure 10).

The southwestern sector of the Mekkam inlier (cross-section I-I'; Figures 10 and 11) is characterized by S0 and S1 trending NE-SW, with gentle to moderate dips to the NW and SE. The intersection lineation L1 trends mostly NW-SE. Along cross-section I-I', the polarity varies: clear reverse polarity criteria (graded bedding) were recognized in the Ayn Serraq area, where the S0/S1 relationships indicate west-vergences (western portion of cross-section I-I'); towards the SE, the opposite stratigraphic polarity and structural relationships were observed, with S0 and S1 folded by a Dc NE-SW trending upright synform (central portion of cross-section I-I'); further to the SE, in the corresponding Dc antiform, the dominant polarity is reverse and D1 structures show NW-vergence, although minor normal limbs locally crop out (eastern portion of cross-section I-I'). Besides the NE-SW highly-dipping crenulation cleavage associated with the macro-scale Dc folds, a second crenulation cleavage oriented NW-SE (Sc1) was also recognized.

In the central and western sectors of the Mekkam inlier (cross-sections J-J' and M-M'; Figures 10 and 11), the S0 trend is variable and dip is usually low. Concerning the D1 folds, L1 is systematically oriented NW-SE, with gentle plunges towards the NW and SE. The western segment of cross-sections J-J' and M-M' is dominated by reverse polarities suggesting the presence of a kilometric-scale overturned D1 limb. Besides local rotations, S1 is generally NW-SE trending and its geometric relationships with S0, together with the asymmetry of the parasitic folds, indicate SW-vergences associated with the overturned limb; the scarce NE-vergences correspond to minor normal limbs. Towards the NE (eastern segment of cross-sections J-J' and M-M'), polarity and local vergence are dominantly the opposite, indicating a D1 normal limb (with NE-vergence). The three sets of crenulation cleavage (Sc1, Sc2, and Sc3; see Section 4.1.2) appear variably developed. The main structural trend (NW-SE) is controlled by Sc1, but in the northern segment of cross-section J-J', dip directions towards the NW were found due to the existence of a WSW-ENE oriented open antiform (Sc2) between El Manjem and El Khemis. The low-dip Sc3 cleavage can be locally very penetrative, especially in cross-section J-J' south of El Manjem mine and in the El Khemis area, where this cleavage often produces tectonic banding that partially obliterates the previous structures. As in other sectors of the region studied, the different sets of

crenulation cleavages do not appear developed together, and, therefore, their mutual relationships are unclear.

The structural trend in the northern sector of the Mekkam inlier (cross-sections K-K' and L-L'; Figures 10 and 11) is dominated by NE-SW (western part) and NW-SE (eastern part) crenulation upright folds. The S1/S0 relationships indicate west-vergences, which, together with reverse polarity criteria, suggest a dominant D1 overturned limb.

In the easternmost sector of the inlier (cross-section N-N', Figures 10 and 11), S0, S1, and L1 are mainly oriented NW-SE due to the presence of Sc1 crenulation folds. In the Dc synform, the stratigraphic polarity is reverse, which, together with the relationship between S1 and S0 showing local SW-vergence, indicates the presence of an overturned limb of a kilometric-scale D1 fold. Opposite relationships and polarities were observed in the corresponding Dc antiform (cross-section N-N', Figure 11).

The DMMS deformed by D1 are unconformably overlain by Visean sediments cropping out in relatively small outcrops in the southern and southeastern parts of the Mekkam inlier (Figure 2). The angular unconformity is well exposed NW of Hassiane Ed Diab (Loukrayma area, Figures 3f and 10) and in a small and tectonized outcrop in the Tafarine area (Figure 10). In both outcrops, the D1 structures do not penetrate into the Visean sediments, which, in turn, are only affected by the NE-SW trending crenulation cleavage (Sc2) observed in the DMMS.

In the Loukrayma area, the Visean unconformity is partially affected by an important WNW-ESE trending semi-brittle shear zone with dextral strike-slip kinematics, which produced a tectonized band of at least 500 m-thick in the DMMS.

4.5 Building up a composite cross-section of the Debdou-Mekkam region

The above descriptions show that the Debdou-Mekkam region is characterized by a series of pre-Late Visean tight to isoclinal, inclined to recumbent, plurikilometric D1 folds (Figure 12) with a related axial-planar main foliation S1. The L1 map delineated in Figure 12 shows important strike variations from NW-SE, through N-S, NE-SW, to E-W, being the relative regional vergence towards the NE, E, SE and S respectively.

In the Debdou inlier (cross-sections 1-1' to 4-4'; Figure 12), the folds are asymmetric with axial surfaces moderately dipping towards the west. The direction of D1 structures changes from NW-SE (cross-section 1-1') to NNE-SSW (cross-sections 2-2' and 3-3'), and then again to NW-SE (cross-section 4-4'). The regional vergence is towards the east, with the normal limbs dominated by normal polarities and local east-vergences while the overturned limbs show reverse polarities and local west-vergences. As a whole, this inlier is characterized by the regular alternation of normal and overturned limbs. The moderately inclined D1 folds in this inlier are scarcely affected by the later Dc deformations.

The D1 Debdou fold train continues towards the east across the Lalla Mimouna-Oued Awam inliers. From the easternmost part of the Debdou inlier to the southwestern part of the Mekkam inlier, a D1 normal limb approximately 30 km-long is reconstructed (cross-section 5-5'; Figure 12). S0 and S1 are mostly subhorizontal, and the stratigraphic polarity dominantly normal. Toward the east, the SW-NE trending upright crenulation folds become more penetrative with a kilometric-scale antiform deforming the previous structures (cross-section 5-5' in Figure 12). Along this plurikilometric D1 normal limb, the structural trend is rotated, from west to east: in the western part L1 is rotated clockwise changing from NW-SE

to E-W; on the contrary, in the eastern part, L1 trend rotates counterclockwise from E-W to NNW-SSE (Figure 12).

The axial surface of the D1 anticline whose c. 30 km-long normal limb crops out in the Lalla Mimouna-Oued Awam inliers, emerges in the SW sector of the Mekkam inlier, where it is folded by SW-NE trending upright crenulation folds (Dc). Here, the D1 normal limb crops out in the core of a Dc synform, and is underlain by a new overturned limb that appears in Dc antiforms located towards the SE and NW (Figure 11). L1 is crenulated by Dc folds and trends SE-NW. Towards the north, this overturned limb appears flat-lying in a wide area west of Lamqam village, maintaining the same L1 trend (western segment of cross-section 6-6', Figure 12). Moreover, just to the north of Lamqam, the axial surface of the D1 anticline dips towards the NE (refolded plunging anticline), thus causing the overlying normal limb to crop out again (eastern segment of cross-section 6-6', Figure 12). Further east, this normal limb is overlain by a new overturned limb, and the axial surface between them is deformed by NW-SE upright crenulation folds (cross-section 7-7', Figure 12). In that sector, L1 maintains the NW-SE trend but, towards the NW, it rotates to N-S and then to SW-NE due to WSW-ENE crenulation folds. Overall, the crenulation deformations are more penetrative in the Mekkam inlier than in the western inliers. Besides the variable development of the low-dipping crenulation cleavage, the occurrence of NE-SW and NW-SE trending upright crenulation folds forms a dome-and-basin-like interference pattern that makes the D1 structure in the Mekkam inlier to be, on average, flat-lying.

5 Discussion

5.1 Age of the Debdou-Mekkam Metasediments

Previous dating of the DMMS based on fossil plant fragments (Médioni, 1980) and palynomorphs (Marhoumi, 1984; Marhoumi et al., 1983) gave Early Carboniferous and Middle-Late Devonian biostratigraphic ages, respectively. Our detrital zircon geochronological study (Section 3.1) constrains the maximum depositional age of the DMMS at Late Devonian (more specifically Famennian) according to the youngest zircon population observed in four of the five samples. Therefore, our U-Pb data indicate that a younger putative age for the DMMS deposition would be compatible with the Early Carboniferous ages deduced from fossil plant fragments, but not with the Middle-Late Devonian ages suggested by palynomorphs, which would probably represent redeposited material. The real depositional age of the DMMS can be constrained by taking into account the series of subsequent events, specifically D1 deformation, emersion, partial erosion, renewed subsidence and unconformable sedimentation of the overlying Late Visean succession, this latter well dated with brachiopods and polyps (Médioni, 1979 and references therein). In our preferred interpretation, the deposition of the DMMS occurred at Late Devonian time (Late Frasnian to Late Famennian), while D1 deformation likely occurred during Early Carboniferous (Tournaisian). Nonetheless, the presence of fossil plant fragments (Médioni, 1980) suggests that the deposition of the DMMS might have continued until the Early Carboniferous. In this case, the D1 deformational event, and the subsequent emersion/erosion would have occurred in a very short time span (1-5 Ma?), i.e. sedimentation would not cease until the Early Tournaisian, while D1 deformation would have occurred during Late Tournaisian-Early Visean time.

A closer examination of the average maximum depositional ages suggests, not without uncertainty, an eastward younging direction (see Figure 2 for sample location): from 375 Ma (2 data from sample DEB2), to 370 Ma (4 data from sample MIM2), and c. 362 Ma

(n = 7, 9 and 4 from samples OUJ10, OUJ11 and OUJ13, respectively). This observation is in accordance with our interpretation that the DMMS represents a fore-arc basin fed by a close active magmatic (zircon-forming) arc, which was probably migrating towards the SE in relation to the subduction of the Rheic oceanic lithosphere underneath an Avalonian promontory (see Sections 5.2 and 5.4). In this scenario, the neo-formed zircons would have been rapidly incorporated into the neighboring fore-arc basin and, therefore, the zircon crystallization ages and the maximum depositional ages of the sediments would be almost coeval. Furthermore, if the sedimentation continued during the Early Tournaisian, the youngest part of the DMMS would have been deposited in a foreland basin fed by the dismantling of the already inactive Devonian magmatic arc.

5.2 Detrital zircon provenance in the Debdou-Mekkam Metasediments

With the exception of the Devonian population, the relevant old inherited detrital zircon populations in the DMMS samples are the prevalent Ediacaran peak (c. 620 Ma), a secondary middle Paleoproterozoic peak (c. 2.1 Ga), and sometimes a Neo-Archean minor population (c. 2.5 Ga; Figure 4). These populations are respectively related to primary sources of Cadomian/Pan-African, Eburnean and Liberian ages, which were formed by successive orogenies in northern Gondwana, and they are globally interpreted as indicative of West African Craton (WAC) affinity (e.g. Nance et al., 2008 and references therein). Recent U-Pb geochronological data on detrital zircons from the Ordovician-Devonian passive margin sequence of the para-autochthonous Eastern Moroccan Meseta (Accotto et al., 2019; Ghienne et al., 2018) highlighted the presence of these detrital zircon populations and inferred their primary WAC affinity. In addition, these studies also found a Tonian-Stenian (c. 1 Ga) population, and a Mesoproterozoic (c. 1.7-1.1 Ga) gap which, considered together, point to NE-Africa secondary sources (Saharan Metacraton and/or Arabian-Nubian Shield), instead of Grenville (Amazonian) sources (Accotto et al., 2019; Ghienne et al., 2018). However, the new data provided in this study include a minor but remarkably continuous zircon content (up to 13.6%) in the c. 0.9-1.9 Ga time span (Figure 4h). Sources of these ages are virtually unknown in the WAC, unless in the Rokelides (De Waele et al., 2015; Villeneuve et al., 2015) and in the Bassarides (Brinckmann and Meinhold, 2007; Villeneuve et al., 2015). Nevertheless, these potential detrital zircon source areas (southern WAC) are a long way from the Eastern Moroccan Meseta and, more importantly, if they were the source of our Mesoproterozoic detrital zircon grains, similar ages would have been encountered also in detrital zircon grains from other Variscan domains located between the source regions and the studied area (e.g. the Anti-Atlas region; Abati et al., 2010; Avigad et al., 2012), which is not the case. On the other hand, c. 0.9-1.9 Ga ages are typical of an Amazonian-type basement, which suggests that the Precambrian zircon inheritance in our samples is from both WAC and Amazonian-type basements, i.e. they contain Gondwanan- and Avalonian-derived detrital zircons. The most plausible explanation for the presence of zircon grains derived from an Amazonian/Avalonian source resides in the commonly accepted paleogeographic attribution of Avalonia as part of northern Gondwana during Neoproterozoic-Cambrian time (Figure 13a), which is prior to its northward Early Paleozoic drift during the opening of the Rheic Ocean (Figure 13b). In fact, Avalonia is thought to have been located in a western position of the northern Gondwana margin during the Neoproterozoic-Cambrian time, and therefore connected not only to the WAC, but also to Amazonia (e.g. Cocks & Fortey, 2009; Linnemann et al., 2012; Murphy et al., 2006).

An outstanding feature of our zircon study is the presence of a Devonian detrital zircon population (c. 360-390 Ma, peak at c. 376 Ma; Figure 4). The content of Devonian

detrital zircons in the analyzed samples is very variable (1.4% in sample DEB2, up to 37% in sample OUJ13), which can be taken as evidence of a nearby and immature (heterogeneous) source, instead of a homogeneous one. Furthermore, the generally almost idiomorphic morphology of the Devonian detrital zircon grains (see Supporting Information) suggests a limited transportation of the sediments, in agreement with a relatively close source.

When considering a source for these Devonian zircon grains, the absence of outcropping igneous rocks of these ages in all NW-Africa must be stressed. The only exception is the Sehoul Block in Western Morocco (Figure 1; see Section 1), where Famennian (c. 367 Ma; U/Pb on igneous zircons) granites are exposed and postdate a presumably middle Paleozoic (Caledonian?) deformation (Tahiri et al., 2010). Just north of the Moroccan Variscides, in SW Iberia, Late Paleozoic metasediments from both the South Portuguese and Ossa-Morena Zones also provided Middle-Late Devonian detrital zircon populations, interpreted as derived from an unexposed magmatic arc, active along the Avalonian convergent margin during the Middle-Late Devonian subduction of the Rheic Ocean (Pereira et al., 2012, 2017; Pérez-Cáceres et al., 2017). Similarly, and based on the comparable ages of the Devonian detrital zircon populations and the paleogeographic vicinity between the Iberian and Moroccan Variscides, we interpret the DMMS as being primarily derived from a Devonian magmatic arc formed in the Avalonian margin, as a consequence of the northward subduction of the Rheic oceanic lithosphere. Furthermore, the hypothesis of a convergent/collisional geodynamic setting, in which the DMMS were deposited, is also supported by the comparison between the Cumulative Probability Plots of our samples and the areas defined by Cawood et al. (2012) for different geodynamic contexts (Figure 4f).

The Hf isotope analyses carried out on the Devonian zircons of the DMMS show a vertical ε_{Hf} array varying from +8.5 to -6.5, with T_{NC} ranging from c. 0.6 Ga to c. 1.6 Ga (Figure 5e). Despite this variability, most ε_{Hf} data are positive and suggest that these zircon grains formed from a magma generated by partial melting of Neoproterozoic continental crust. Nevertheless, some interaction with older Mesoproterozoic continental basement might also have occurred, which would account for the older model ages (T_{NC}) and the slight negative ε_{Hf} values recorded in MIM2. Very similar results were obtained by Pereira et al. (2017) in the Devonian zircon grains from SW Iberia (Figure 14a). Furthermore, the comparison between the Hf isotopic signature of our older data (> 450 Ma; Figure 14b) with those from Avalonian terranes (Henderson et al., 2018 and references therein) and the WAC (Abati et al., 2012; Avigad et al., 2012) shows similar distributions of the Ediacaran-Cryogenian (c. 620 Ma) and Paleoproterozoic (c. 2.1 Ga) main detrital zircon populations, suggesting that these terranes had a common evolution in North Gondwana (including both the Cadomian and Eburnean orogenies). The quite abundant Mesoproterozoic population in Avalonia, which is absent in the WAC (gap between c. 1.1 and 1.8 Ga), shows the majority of ε_{Hf} values between c. +10 and c. -10, being many of them slightly positive (from c. +5 to c. 0); a comparable distribution is found in our samples (Figure 14b), indicating that an Avalonia-type basement could have supplied detrital zircons to the DMMS.

As a whole, our Hf isotope data provide additional evidence for the deposition of the DMMS in a fore-arc (and/or foreland) geological setting fed by both the north Gondwanan margin (WAC source) and a Devonian magmatic arc built on a Neoproterozoic crustal basement that included subordinate Mesoproterozoic Avalonia-derived igneous rocks. In this respect, both the Sehoul Block and the South Portuguese Zone are considered Avalonia-derived terranes (Michard et al., 2010; Pérez-Cáceres et al., 2017; Simancas et al., 2005; Tahiri et al., 2010 and references therein), i.e. they are nearby examples of a source type for the DMMS, which would include a Middle-Late Devonian continental magmatic arc with the Avalonian basement.

5.3 Original vergence of D1 folds

Our structural study focused on D1 folds across the investigated region (Section 4). The structural map in Figure 12 shows a complicated pattern for the trends of L1 intersection lineation (S0/S1) and the inferred axial traces of D1 folds (see Section 4.5 for a summary of D1 trends and Dc interference patterns). The simplified trend of D1 folds changes from NNW-SSE in the Debdou inlier, with ENE-vergence, to E-W in the Lalla Mimouna-Oued Awam inliers, with S-vergence, and, finally, to NW-SE in the Mekkam inlier, with NE-vergence, depicting an apparent clockwise rotation between the Debdou and Lalla Mimouna-Oued Awam inliers and a counterclockwise one between the latter and the Mekkam inlier (sketch in Figure 12). Accordingly, the local vergence on the D1 normal limbs is towards the ENE in the Debdou inlier, towards the south in the Lalla Mimouna-Oued Awam inliers, and towards the NE in the Mekkam inlier (grey arrows in the sketch in Figure 12). The pronounced curved trend of D1 folds, if restored to an original straight orientation, results in an average SW-NE trend with SE vergence on the normal limbs (sketch in Figure 12). We interpret that most of the present-day curvature of D1 folds is due to the post-Visean upright crenulation folds (Dc), as observed in some sectors of the Mekkam inlier (Figure 10). However, part of the curved trend of D1 folds might be primary, i.e. D1 folds could have been formed with an oscillatory trend that was later tightened by the upright crenulation folds. The reason for this putative primary undulated fold pattern is uncertain, although it can be speculated that the arcuate edge (at scale of tens of kilometers) of a southeastward-pushing crustal block could have formed a slightly curved D1 fold belt (see section 5.4).

5.4 Proposing a large-scale plate tectonic scenario

The Moroccan Variscides are generally viewed as an intracontinental part of the Variscan-Alleghanian orogenic system, developed on the northern Gondwanan margin and constituted by a number of tectonic domains bounded by crustal-scale strike-slip shear zones (e.g. Hoepffner et al., 2005, 2006; Michard et al., 2010). The absence of ophiolitic rocks and high-pressure belts seems to support this interpretation. However, the presence of Devonian granites, which postdate the ductile (seemingly Caledonian) deformation observed in the Sehoul Block, suggests a non-Gondwanan origin for this domain and points to a cryptic suture, namely the Rheic Ocean suture, between itself and the rest of the Moroccan Variscides (e.g. Hoepffner et al., 2005; Michard et al., 2010 and references therein; Simancas et al., 2005; Tahiri et al., 2010). To the south, this cryptic suture has also been inferred in the Souttoufides (western Saharan belts; Figure 1a), by the recognition of "exotic" (Laurentian-derived) terranes (e.g. Gärtner et al., 2013; Villeneuve et al., 2015), and in the Mauritanides (the southernmost outcropping transect of the Variscan-Alleghanian orogenic system in Africa; e.g. Villeneuve, 2008; Villeneuve et al., 2010). To the north, the Rheic Ocean suture is masked in SW Iberia at the boundary between the Ossa Morena Zone and the South Portuguese Zone (e.g. Braid et al., 2011; Pérez-Cáceres et al., 2015, 2017). Further north, the identification of the Rheic Ocean suture in the allochthonous complexes of NW Iberia is uncertain (e.g. Arenas et al., 2014; Martínez Catalán et al., 2019).

The flysch nature (turbidites with coarse-grained greywackes), great thickness (more than 10 km according to an approximate restoration of our synthetic cross-section in Figure 12) and intense deformation (D1 folding accounting for important tectonic shortening) that characterize the Late Devonian-earliest Carboniferous DMMS have no equivalent in nearby Paleozoic inliers of the Eastern Moroccan Meseta. In this area (Beni Snassene, Oujda, and

Jerada inliers; Figure 1b), a relatively thin pre-Carboniferous passive margin sequence is weakly deformed, together with the overlying Early Carboniferous succession, by E-W upright open folds. Furthermore, the deformation decreases to the west and southwest: in the Western Moroccan Meseta, NW- to NNE-trending upright folds associated with spaced cleavage and low- to very low-grade metamorphism were described, together with NNE-SSW transtensional basins, while the Coastal Block is characterized by NNE-trending upright open folds and no metamorphism (Hoepffner et al., 2006).

The Moroccan Meseta at Ordovician-Devonian time was part of the northwestern continental passive margin of Gondwana with the Rheic Ocean developed to the N and NW (Figure 13b). The counterpart was the Laurussia continental margin, which resulted from the middle Paleozoic Caledonian-Acadian collision between Avalonia and Laurentia-Baltica. The subduction of the Rheic Ocean began at Middle Devonian time and a magmatic arc formed along the Avalonian margin (Nance et al., 2010, 2012; Pereira et al., 2017). The subduction continued during Late Devonian (Figure 15a) with the partial closure of the Rheic Ocean at the frontal part of an Avalonian promontory (Simancas et al., 2005; Figure 15b). At the Famennian (and Tournaisian?) time, the Late Devonian magmatic arc and its Avalonian basement experienced denudation giving way to thick turbiditic flysch sedimentation (e.g. DMMS) took place in a basin located in the fore-arc region, and likely attesting the oceanic trench that separated the Avalonian magmatic arc from the Gondwana continental passive margin (Figure 15b). The sediments were supplied mainly by erosion of the adjacent upper plate (Avalonian basement and its Middle-Late Devonian magmatic arc), but mature detritus could have also been provided from the WAC as pointed out by the presence of a relatively important Paleoproterozoic detrital zircon population, which is less abundant in Avalonian terranes. The advance of the Avalonian front towards the SE might have produced the coeval migration of the depocenter in the DMMS basin throughout the Famennian.

At Early Carboniferous time (Tournaisian-Early Visean), continued convergence between the Avalonian promontory and Gondwana cut sediment supply to the DMMS basin and triggered compressive collisional deformation (D1 folding; Figure 15c). Thus, km-scale NE-SW trending SE-verging inclined to recumbent folds formed due to the south-eastward pushing of the overriding Avalonian promontory located to the NW of the DMMS basin. The geometry and outcropping (visible) size of the D1 fold belt (Figure 12) entails a considerable NW-SE shortening that implies the existence of a basal detachment between the folded belt and its relative para-autochthonous, which is the passive margin sequence of North Gondwana exposed in the neighbouring inliers (Beni Snassene, Oujda; Figure 1b). Unfortunately, the D1 deformation front and the transition to its relative Gondwanan foreland are not exposed.

The low- to very low-metamorphic grade of the DMMS suggests that these rocks never reached deep orogenic conditions and thus D1 deformation occurred at a relatively high structural level, i.e. the DMMS were not deeply underthrust below the Avalonian crust. Furthermore, the age of the Eo-Variscan metamorphic event proposed by Huon et al. (1987) based on K-Ar analyses of allegedly metamorphic illite grains from the Debdou and Mekkam inliers (372.3 ± 8.1 Ma and 368.3 ± 7.9 Ma, respectively) is overestimated according to our detrital zircon ages. These ages are older than, or coeval with, the maximum depositional ages of the DMMS deduced from the youngest detrital zircon population. We suggest that D1 occurred shortly after the deposition of the DMMS, in accordance with the proposed continued southeastwards advance of the adjacent Avalonian promontory. Furthermore, D1 occurred before the formation of the Visean unconformity, since the Late Visean sediments were not affected by this deformational event. Therefore, D1 should have occurred at Tournaisian-Early Visean time.

Concerning the Avalonian nature of the continental promontory that collided with the Gondwanan margin (Figure 13c) to generate the SE-verging km-scale D1 folds in the Eastern Moroccan Meseta, the existence of neighbouring terranes interpreted as Avalonian derived supports our model. To the north, in SW Iberia, Devonian detrital zircons were interpreted as remnants of a missing subduction-related (Avalonian?) magmatic arc (Pereira et al., 2012), while the South Portuguese Zone is considered part of the Avalonian terrane (Pérez-Cáceres et al., 2017 and references therein), and its boundary with the adjacent Ossa-Morena Zone hides the Rheic suture (Pérez-Cáceres et al., 2015, 2016). The dominant left-lateral kinematics along the Ossa-Morena-South Portuguese Zone boundary agrees with the paleogeographic location of SW Iberia on the northern side of the Avalonian salient (Figure 15c). The southern side of that promontory would be represented by the Caledonian Sehoul Block (Figure 15c; Simancas et al., 2005; Tahiri et al., 2010), where a Late Carboniferous brittle thrust would have obliterated previous right-lateral kinematics concomitant to the left-lateral one occurred in SW Iberia. In-between SW Iberia and the Sehoul Block, the southeastwards frontal impingement of the Avalonian promontory would have produced the km-scale SE-vergent recumbent folds in the Eastern Moroccan Meseta.

To sum up, the Early Carboniferous collisional deformation and detrital zircon isotopic data (U-Pb and Hf) recorded by the DMMS provide with indirect evidence on the location of a cryptic Rheic Ocean suture in the Eastern Moroccan Meseta, separating Avalonia and northern Gondwana (Figure 13c). In this context, correlations with other suture contacts can be proposed in an attempt to reconstruct the large-scale Variscan scenario. To the west of the Eastern Moroccan Meseta, the suture would continue concealed by the thrust of the Sehoul Block onto the Western Moroccan Meseta (Tahiri et al., 2010) and, further south, in the Souttoufides and, perhaps, the Mauritanides (Villeneuve et al., 2015). To the north of the Eastern Moroccan Meseta, the Rheic Ocean suture appears blurred in SW Iberia (Pérez-Cáceres et al., 2015), and prolongs between SW England and other European Variscan Massifs in France, Belgium, Germany and Czech Republic (e.g. Franke et al., 2017; Martínez Catalán et al., 2019; Shail & Leveridge, 2009).

6 Conclusions

The DMMS constitutes a low- to very low-grade intensely deformed siliciclastic succession, previously attributed to either Middle-Late Devonian or Early Carboniferous ages. New U-Pb ages on detrital zircons constrain the maximal depositional age at Late Devonian and, therefore, are compatible with Early Carboniferous deposition. However, the fact that the DMMS underwent the main deformational event (D1) prior to the deposition of the unconformable Upper Visean sediments, together with the euhedral morphologies of the Devonian detrital zircons, points to deposition at Late Devonian time (or no later than Early Tournaisian) and subsequent deformation at Early Carboniferous time (Tournaisian-Early Visean).

Apart from the Late Devonian detrital zircon population, the DMMS shows the common presence of Ediacaran and Paleoproterozoic populations compatible with a northern WAC source. Furthermore, a conspicuous amount of scattered grains with ages between 1.9 Ga and 0.9 Ga evokes the possibility of an exotic source that might be found in the basement of an Avalonian promontory approaching the northern margin of Gondwana during the closure of the Rheic Ocean at Late Devonian time. These Avalonia-derived terranes crop out in the South Portuguese Zone in SW Iberia, and in the Sehoul Block in NW Morocco. Furthermore, the Hf isotopic signature of the Devonian detrital zircons suggests that they

might be sourced in a subduction related magmatic arc located on the Avalonian margin, in which reworking of Neo- and Mesoproterozoic Avalonian crust would have occurred. Thus, the DMMS would represent turbiditic deposits in a fore-arc (and/or foreland) basin.

The deformational events that affected the Debdou-Mekkam massif are: (i) a main D1 event characterized by tight to isoclinal folds and slaty cleavage, with regional NE-SW trend and SE vergence, which occurred at Early Carboniferous (probably Tournaisian) time; and (ii) a late Dc event (or events) responsible for upright open to tight folds and crenulation cleavage, which affected both the DMMS and the overlying Upper Visean succession. The main deformation D1 accounts for regional shortening that occurred during the first phases of the collision between the northern passive margin of Gondwana and an Avalonian promontory. In this scenario, the Avalonian block over-thrusted the Gondwanan margin, giving way to the SE-verging D1 structures. Therefore, the DMMS attests to sedimentation related to the denudation of a missing Late Devonian magmatic arc and subsequent Early Carboniferous collisional deformation triggered by an Avalonian promontory that approached the Gondwana margin after the consumption of the Rheic Ocean lithosphere. In this context, the DMMS might represent a syn-orogenic Eo-Variscan basin witnessing the cryptic oceanic suture between Avalonia and Gondwana in the Eastern Moroccan Meseta.

Acknowledgments

This study was founded by the Ministerio de Economía y Competitividad (MINECO) of Spain through the project PANGEATOR (CGL2015-71692-P) and the Doctoral scholarship BES-2016-078168. GeoHistory Facility instruments were funded via an Australian Geophysical Observing System grant provided to AuScope Pty Ltd. by the AQ44 Australian Education Investment Fund program. The NPII multi-collector was obtained via funding from the Australian Research Council LIEF program (LE150100013). The authors want to express their gratitude to Dr. Manuel Francisco Pereira (University of Évora, Portugal) and Dr. Michel Villeneuve (Centre Européen de Recherche et d'Enseignement des Géosciences de l'Environnement, France) for their constructive reviews that helped to improve the quality of the original manuscript. Special thanks to Brad McDonald (Curtin University, Australia) for technical assistance regarding LA-ICPMS and Hf analyses, Profs. Abdelfatah Tahiri (University Mohammed V of Rabat, Morocco) and Hassan El Hadi (University Hassan II of Casablanca, Morocco) for their support during field work, Prof. Yvette Kuiper (Colorado School of Mines, USA) for her precious hints about the interpretation of Hf data, and Dr. Lorenzo Valetti for proof reading the manuscript.

Supporting information can be obtained in Mendeley Data:
http://dx.doi.org/10.17632/b8fdbykmbx.1
(https://data.mendeley.com/datasets/b8fdbykmbx/draft?a=eaae2da0-8e22-4056-861b-4824984f1c10).

References

Abati, J., Aghzer, A.M., Gerdes, A., & Ennih, N. (2012). Insights on the crustal evolution of the West African Craton from Hf isotopes in detrital zircons from the Anti-Atlas belt. *Precambrian Research* 212–213, 263–274. doi:10.1016/j.precamres.2012.06.005

Abati, J., Mohsine Aghzer, A., Gerdes, A., & Ennih, N. (2010). Detrital zircon ages of Neoproterozoic sequences of the Moroccan Anti-Atlas belt. *Precambrian Research*, *181*(1–4), 115–128. https://doi.org/10.1016/j.precamres.2010.05.018

Accotto, C., Martínez Poyatos, D. J., Azor, A., Talavera, C., Evans, N. J., Jabaloy-Sánchez, A., et al. (2019). Mixed and recycled detrital zircons in the Paleozoic rocks of the Eastern Moroccan Meseta: Paleogeographic inferences. *Lithos*. https://doi.org/10.1016/j.lithos.2019.04.011

Avigad, D., Gerdes, A., Morag, N., & Bechstädt, T. (2012). Coupled U-Pb-Hf of detrital zircons of Cambrian sandstones from Morocco and Sardinia: Implications for provenance and Precambrian crustal evolution of North Africa. *Gondwana Research*, *21*(2–3), 690–703. https://doi.org/10.1016/j.gr.2011.06.005

Arenas, R., Díez Fernández, R., Sánchez Martínez, S., Gerdes, A., Fernández-Suárez, J., & Albert, R. (2014). Two-stage collision: Exploring the birth of Pangea in the Variscan terranes. *Gondwana Research*, 25(2), 756–763. https://doi.org/10.1016/j.gr.2013.08.009

Azor, A., Rubatto, D., Simancas, J.F., González Lodeiro, F., Martínez Poyatos, D., Martin Parra, L.M., & Matas, J. (2008). Rheic Ocean ophiolitic remnants in southern Iberia questioned by SHRIMP U-Pb zircon ages on the Beja-Acebuches amphibolites. *Tectonics* 27, 1–11. doi:10.1029/2008TC002306

Bell, A. M. (1981). Vergence: an evaluation. *Journal of Structural Geology*, 3(3), 197–202. https://doi.org/10.1016/0191-8141(81)90015-8

Blichert-Toft, J., & Albarède, F. (1997). The Lu-Hf isotope geochemistry of chondrites and the evolution of the mantle-crust system. *Earth and Planetary Science Letters*, *148*(1–2), 243–258. https://doi.org/10.1016/S0012-821X(97)00040-X

Brinckmann, J., & Meinhold, K.-D. (2007). *La géologie de la Chaîne des Bassarides et des terrains environnants au Nord-Ouest de la Guinée: avec 16 tableaux, 5 annexes*. Schweizerbart.

Bouvier, A., Vervoort, J. D., & Patchett, P. J. (2008). The Lu–Hf and Sm–Nd isotopic composition of CHUR: Constraints from unequilibrated chondrites and implications for the bulk composition of terrestrial planets. *Earth and Planetary Science Letters*, *273*(1–2), 48–57. https://doi.org/10.1016/j.epsl.2008.06.010

Braid, J.A., Murphy, J.B., Quesada, C., & Mortensen, J. (2011). Tectonic escape of a crustal fragment during the closure of the Rheic Ocean: U-Pb detrital zircon data from the Late Palaeozoic Pulo do Lobo and South Portuguese zones, southern Iberia. *Journal of the Geological Society of London*. 168, 383–392. doi:10.1144/0016-76492010-104

Cawood, P. A., Hawkesworth, C. J., & Dhuime, B. (2012). Detrital zircon record and tectonic setting. *Geology*, *40*(10), 875–878. https://doi.org/10.1130/G32945.1

Chu, N.-C., Taylor, R. N., Chavagnac, V., Nesbitt, R. W., Boella, R. M., Milton, J. A., et al. (2002). Hf isotope ratio analysis using multi-collector inductively coupled plasma mass spectrometry: an evaluation of isobaric interference corrections. *Journal of Analytical Atomic Spectrometry*, 17(12), 1567–1574. https://doi.org/10.1039/b206707b

Clauer, N., Jeannette, D., & Tisserant, D. (1980). Datation isotopique des cristallisations successives d'un socle cristallin et cristallophyllien (Haute Moulouya, Moyen Maroc). *Geologische Rundschau*, *69*(1), 63–83. https://doi.org/10.1007/BF01869024

Cocks, L. R. M., & Fortey, R. A. (2009). Avalonia: a long-lived terrane in the Lower Palaeozoic? *Geological Society, London, Special Publications*, *325*(1), 141–155. https://doi.org/10.1144/SP325.7

Desteucq, C., & Fournier-Vinas, C. (1981). Présence d'Ordovicien dans la règion d'Oujda. *Mines, Géologie et Energie*, *50*.

De Waele, B., Lacorde, M., Vergara, F., & Chan, G. (2015). New insights on proterozoic tectonics and sedimentation along the peri-Gondwanan West African margin based on zircon U–Pb SHRIMP geochronology. *Precambrian Research* 259, 156–175. doi:10.1016/j.precamres.2014.08.008

Dewey, J., & Bird, J. (1971). Origin and emplacement of the ophiolite suite: Appalachian ophiolites in Newfoundland. *Journal of Geophysical Research*, *76*(14), 3179–3206. https://doi.org/10.1029/JB076i014p03179

Dhuime, B., Hawkesworth, C., & Cawood, P. (2011). When Continents Formed. *Science*, *331*(6014), 154–155. https://doi.org/10.1126/science.1201245

Díez Fernández, R., & Arenas, R. (2015). The Late Devonian Variscan suture of the Iberian Massif: a correlation of high-pressure belts in NW and SW Iberia. *Tectonophysics*, *654*, 96–100. https://doi.org/10.1016/J.TECTO.2015.05.001

El Hadi, H., Tahiri, A., & Reddad, A. (2003). Les granitoïdes hercyniens post-collisionnels du Maroc oriental : une province magmatique calco-alcaline à shoshonitique. *Comptes Rendus Geoscience*, *335*(13), 959–967. https://doi.org/10.1016/j.crte.2003.09.003

El Hadi, H., Simancas, J. F., Tahiri, A., Gonzalez-Lodeiro, F., Azor, A., & Martinez Poyatos, D. (2006). Comparative review of the Variscan granitoids of Morocco and Iberia: proposal of a broad zonation. *Geodinamica Acta*, *19*(2), 103–116. https://doi.org/10.3166/ga.19.103-116

El Haibi, H., El Hadi, H., Tahiri, A., Martínez Poyatos, D.J., Gasquet, D., Pérez-Cáceres, I., et al. (2020). Geochronology and isotopic geochemistry of Ediacaran high-K calc-alkaline felsic volcanism: An example of a Moroccan perigondwanan (Avalonian?) remnant in the El Jadida horst (Mazagonia). *Journal of African Earth Science*, doi:10.1016/j.jafrearsci.2019.103669

El Hassani, A., Tahiri, A., & Walliser, O. H. (2003). The Variscan Crust between Gondwana and Baltica. *CFS Courier Forschungsinstitut Senckenberg*, (242), 81–87.

El Houicha, M., Pereira, M. F., Jouhari, A., Gama, C., Ennih, N., Fekkak, A., et al. (2018). Recycling of the Proterozoic crystalline basement in the Coastal Block (Moroccan Meseta): new insights for understanding the geodynamic evolution of the northern peri-Gondwanan realm. *Precambrian Research*, *306*(March 2017), 129–154. https://doi.org/10.1016/j.precamres.2017.12.039

Faryad, S. W., & Kachlik, V. (2013). New evidence of blueschist facies rocks and their geotectonic implication for Variscan suture(s) in the Bohemian Massif. *Journal of Metamorphic Geology*, *31*(1), 63–82. https://doi.org/10.1111/jmg.12009

Franke, W., Cocks, L. R. M., & Torsvik, T. H. (2017). The Palaeozoic Variscan oceans revisited. *Gondwana Research*, *48*, 257–284. https://doi.org/10.1016/j.gr.2017.03.005

Gärtner, A., Villeneuve, M., Linnemann, U., El Archi, A., & Bellon, H. (2013). An exotic terrane of Laurussian affinity in the Mauritanides and Souttoufides (Moroccan Sahara). *Gondwana Research*, *24*(2), 687–699. https://doi.org/10.1016/j.gr.2012.12.019

Ghienne, J. F., Benvenuti, A., El Houicha, M., Girard, F., Kali, E., Khoukhi, Y., et al. (2018). The impact of the end-Ordovician glaciation on sediment routing systems: a case study from the Meseta (northern Morocco). *Gondwana Research*, *63*, 169–178. https://doi.org/10.1016/j.gr.2018.07.001

Henderson, B.J., Collins, W.J., Brendan Murphy, J., & Hand, M. (2018). A hafnium isotopic record of magmatic arcs and continental growth in the Iapetus Ocean: The contrasting evolution of Ganderia and the peri-Laurentian margin. *Gondwana Research* 58, 141–160. doi:10.1016/j.gr.2018.02.015

Hoepffner, C. (1977). Données nouvelles sur le Paléozoïques de la bordure occidentale du massif du Tazekka. *Comptes Rendus de l'Académie des Sciences de Paris*, *284*(D), 1635–1637.

Hoepffner, C. (1987). *La tectonique hercynienne dans l'Est du Maroc*. Université Louis Pasteur, Strasbourg.

Hoepffner, C. (1989). L'évolution structurale hercynienne de la Méséta marocain orientale. Essai de mise au point. *Notes & Memoires Du Service Géologique Du Maroc*.

Hoepffner, C., Houari, M. R., & Bouabdelli, M. (2006). Tectonics of the North African Variscides (Morocco, western Algeria): an outline. *Comptes Rendus - Geoscience*, *338*(1–2), 25–40. https://doi.org/10.1016/j.crte.2005.11.003

Hoepffner, C., Soulaimani, A., & Piqué, A. (2005). The Moroccan Hercynides. *Journal of African Earth Sciences*, *43*(1–3), 144–165. https://doi.org/10.1016/j.jafrearsci.2005.09.002

Huon, S., Piqué, A., & Clauer, N. (1987). Étude de l'orogenèse hercynienne au Maroc par la datation K-Ar de l'évolution métamorphique de schistes ardoisiers. *Sciences Géologiques, bulletins et mémoires*, *40*(3), 273–284.

Jackson, S.E., Pearson, N.J., Griffin, W.L. & Belousova, E.A. (2004). The application of laser ablation-inductively coupled plasma-mass spectrometry to in situ U–Pb zircon geochronology. *Chemical Geology*, 211, 47–69. https://doi.org/10.1016/j.chemgeo.2004.06.017

Letsch, D., El Houicha, M., von Quadt, A., & Winkler, W. (2018). A missing link in the peri-Gondwanan terrane collage: the Precambrian basement of the Moroccan Meseta and its lower Paleozoic cover. *Canadian Journal of Earth Sciences*, *55*(1), 1–19. https://doi.org/10.1139/cjes-2017-0086

Linnemann, U., Herbosch, A., Liégeois, J. P., Pin, C., Gärtner, A., & Hofmann, M. (2012). The Cambrian to Devonian odyssey of the Brabant Massif within Avalonia: A review with new zircon ages, geochemistry, Sm-Nd isotopes, stratigraphy and palaeogeography. *Earth-Science Reviews*, *112*(3–4), 126–154. https://doi.org/10.1016/j.earscirev.2012.02.007

Marhoumi, M. R. (1984). *Etude palynologique des séries dinantiennes de la Méséta marocaine. Conséquences stratigraphiques et structurales*. Université Louis Pasteur, Strasbourg.

Marhoumi, M. R., Hoepffner, C., Doubinger, J., & Rauscher, R. (1983). Données nouvelles

sur l'histoire hercynienne de la Meseta orientale au Maroc: l'âge dévonien des schistes de Debdou et du Mekkam. *Comptes Rendus de l'Académie Des Sciences de Paris*, *297*(II), 69–72.

Martínez Catalán, J.R., Collett, S., Schulmann, K., Aleksandrowski, P., & Mazur, S. (2019). Correlation of allochthonous terranes and major tectonostratigraphic domains between NW Iberia and the Bohemian Massif, European Variscan belt. *International Journal of Earth Science*. doi:10.1007/s00531-019-01800-z

Martínez Catalán, J. R., Díaz García, F., Arenas, R., Abati, J., Castiñeiras, P., González Cuadra, P., et al. (2002). Thrust and Detachment systems in the Ordenes Complex (northwestern Spain): implications for the Variscan-Appalachian geodynamics. In J. R. Martínez Catalán, R. D. Hatcher Jr., R. Arenas, & F. Díaz García (Eds.), *Variscan-Appalachian dynamics: the building of the Late Paleozoic basement* (pp. 163–182). Geological Society of America, Special Paper 364.

Matte, P. (2001). The Variscan collage and orogeny (480-290 Ma) and the tectonic definition of the Armorica microplate: a review. *Terra Nova*, *13*(2), 122–128. https://doi.org/10.1046/j.1365-3121.2001.00327.x

Médioni, R. (1979). Carte géologique du Maroc au 1/100.000. Feuille Hassiane Ed Diab. Notice explicative. *Notes et Memoires Du Service Géologique Du Maroc*, *227*(bis), 64.

Médioni, R. (1980). Mise au point stratigraphique sur les terrains carbonifères de la bordure septentrionale des Hauts-Plateaux marocains (massifs de Debdou, boutonnières de Lalla-Mimouna et du Mekam). *Notes Du Service Géologique Du Maroc*, *285*(41), 25–37.

Michard, A., Saddiqi, O., Chalouan, A., & Frizon de Lamotte, D. (2008). *Continental evolution: the geology of Morocco*. (S. Bhattacharji, H. J. Neugebauer, J. Reitner, & K. Stüwe, Eds.). Springer. https://doi.org/10.1007/978-3-540-75761-0

Michard, A., Soulaimani, A., Hoepffner, C., Ouanaimi, H., Baidder, L., Rjimati, E. C., & Saddiqi, O. (2010). The South-Western Branch of the Variscan Belt: evidence from Morocco. *Tectonophysics*, *492*(1–4), 1–24. https://doi.org/10.1016/j.tecto.2010.05.021

Morel, M. L. A., Nebel, O., Nebel-Jacobsen, Y. J., Miller, J. S., & Vroon, P. Z. (2008). Hafnium isotope characterization of the GJ-1 zircon reference material by solution and laser-ablation MC-ICPMS. *Chemical Geology*, 255(1–2), 231–235. https://doi.org/10.1016/j.chemgeo.2008.06.040

Murphy, J. B., Gutiérrez-Alonso, G., Nance, R. D., Fernandez-Suarez, J., Keppie, J. D., Quesada, C., et al. (2006). Origin of the Rheic Ocean: rifting along a Neoproterozoic suture? *Geology*, *34*, 325–328. https://doi.org/10.1130/G22068.1

Murphy, J.B., Quesada, C., Gutiérrez-Alonso, G., Johnston, S.T., & Weil, A. (2016). Reconciling competing models for the tectono-stratigraphic zonation of the Variscan orogen in Western Europe. *Tectonophysics* 681, 209–219. doi:10.1016/j.tecto.2016.01.006

Nance, R. D., Gutiérrez-Alonso, G., Keppie, J. D., Linnemann, U., Murphy, J. B., Quesada, C., et al. (2010). Evolution of the Rheic Ocean. *Gondwana Research*, *17*(2–3), 194–222. https://doi.org/10.1016/j.gr.2009.08.001

Nance, R. D., Gutiérrez-Alonso, G., Keppie, J. D., Linnemann, U., Murphy, J. B., Quesada, C., et al. (2012). A brief history of the Rheic Ocean. *Geoscience Frontiers*, *3*(2), 125–135. https://doi.org/10.1016/j.gsf.2011.11.008

Nance, R. D., Murphy, J. B., Strachan, R. A., Keppie, J. D., Gutiérrez-Alonso, G., Fernández-Suárez, J., et al. (2008). Neoproterozoic-early Palaeozoic tectonostratigraphy and palaeogeography of the peri-Gondwanan terranes: Amazonian v. West African connections. *Geological Society, London, Special Publications*, *297*(1), 345–383. https://doi.org/10.1144/SP297.17

Ouabid, M., Ouali, H., Garrido, C.J., Acosta-Vigil, A., Román-Alpiste, M.J., Dautria, J.M., et al. (2017). Neoproterozoic granitoids in the basement of the Moroccan Central Meseta: Correlation with the Anti-Atlas at the NW paleo-margin of Gondwana. *Precambrian Research*, 299, 34–57. doi:10.1016/j.precamres.2017.07.007

Patchett, P. J., & Tatsumoto, M. (1980). Hafnium isotope variations in oceanic basalts. *Geophysical Research Letters*, 7(12), 1077–1080. https://doi.org/10.1029/GL007i012p01077

Paton, C., Hellstrom, J., Paul, B., Woodhead, J., & Hergt, J. (2011). Iolite: Freeware for the visualisation and processing of mass spectrometric data. *Journal of Analytical Atomic Spectrometry*, 26(12), 2508. https://doi.org/10.1039/c1ja10172b

Pereira, M. F., Chichorro, M., Johnston, S. T., Gutiérrez-Alonso, G., Silva, J. B., Linnemann, U., et al. (2012). The missing Rheic Ocean magmatic arcs: provenance analysis of Late Paleozoic sedimentary clastic rocks of SW Iberia. *Gondwana Research*, *22*(3–4), 882–891. https://doi.org/10.1016/j.gr.2012.03.010

Pereira, M. F., El Houicha, M., Aghzer, A., Silva, J.B., Linnemann, U., & Jouhari, A., 2014. New U-Pb zircon dating of Late Neoproterozoic magmatism in Western Meseta (Morocco). *Gondwana*, 15 - North meets South 133. doi:10.13140/2.1.2651.2641

Pereira, M. F., El Houicha, M., Chichorro, M., Armstrong, R., Jouhari, A., El Attari, A., et al. (2015). Evidence of a Paleoproterozoic basement in the Moroccan Variscan Belt (Rehamna Massif, Western Meseta). *Precambrian Research*, 268, 61–73. doi:10.1016/j.precamres.2015.07.01

Pereira, M. F., Gutíerrez-Alonso, G., Murphy, J. B., Drost, K., Gama, C., & Silva, J. B. (2017). Birth and demise of the Rheic Ocean magmatic arc(s): Combined U–Pb and Hf isotope analyses in detrital zircon from SW Iberia siliciclastic strata. *Lithos*, *278–281*, 383–399. https://doi.org/10.1016/j.lithos.2017.02.009

Pérez-Cáceres, I., Martínez Poyatos, D., Simancas, J. F., & Azor, A. (2015). The elusive nature of the Rheic Ocean suture in SW Iberia. *Tectonics*, *34*(12), 2429–2450. https://doi.org/10.1002/2015TC003947

Pérez-Cáceres, I., Martínez Poyatos, D., Simancas, J. F., & Azor, A. (2017). Testing the Avalonian affinity of the South Portuguese Zone and the Neoproterozoic evolution of SW Iberia through detrital zircon populations. *Gondwana Research*, *42*, 177–192. https://doi.org/10.1016/j.gr.2016.10.010

Pérez-Cáceres, I., Simancas, J. F., Martínez Poyatos, D., Azor, A., & González Lodeiro, F. (2016). Oblique collision and deformation partitioning in the SW Iberian Variscides. *Solid Earth*, *7*(3), 857–872. https://doi.org/10.5194/se-7-857-2016

Piqué, A. (1994). *Géologie du Maroc*. Marrakech: éditions Pumag.

Piqué, A. (2001). *Geology of Northwest Africa*. Berlin: Borntraeger.

Piqué, A., & Michard, A. (1981). Les zones structurales du Maroc hercynien. *Sciences Géologiques, Bulletins et Mémoires*, *34*(2), 135–146.

Piqué, A., & Michard, A. (1989). Moroccan Hercynides: a synopsis. The Paleozoic sedimentary and tectonic evolution at the northern margin of West Africa. *American Journal of Science*, *289*, 286–330.

Rauscher, R., Marhoumi, R., Vanguestaine, M., & Hoepffner, C. (1984). Datation palynologique des schistes du Tazekka au Maroc. Hypothèse structurale sur la socle hercynien de la Meseta orientale. *Comptes Rendus de l'Académie Des Sciences de Paris*, *294*(II), 1203–1206.

Romer, R. L., & Kroner, U. (2019). First direct evidence for a contiguous Gondwana shelf to the south of the Rheic Ocean. *Geology*, *47*(8), 767–770. https://doi.org/10.1130/G46255.1

Scherer, E., Münker, C., & Mezger, K. (2001). Calibration of the Lutetium-Hafnium Clock. *Science*, *293*(5530), 683–687. https://doi.org/10.1126/science.1061372

Schulmann, K., Lexa, O., Janoušek, V., Lardeaux, J. M., & Edel, J. B. (2014). Anatomy of a diffuse cryptic suture zone: An example from the Bohemian Massif, European Variscides. *Geology*, *42*(4), 275–278. https://doi.org/10.1130/G35290.1

Shail, R.K. & Leveridge, B.E. (2009). The Rhenohercynian passive margin of SW England: Development, inversion and extensional reactivation. *Comptes Rendus Geoscience* 341, 140–155. doi:10.1016/j.crte.2008.11.002

Simancas, J. F., Azor, A., Martínez Poyatos, D., Tahiri, A., El Hadi, H., González-Lodeiro, F., et al. (2009). Tectonic relationships of Southwest Iberia with the allochthons of Northwest Iberia and the Moroccan Variscides. *Comptes Rendus Geoscience*, *341*(2–3), 103–113. https://doi.org/10.1016/j.crte.2008.11.003

Simancas, J. F., Tahiri, A., Azor, A., Lodeiro, F. G., Martínez Poyatos, D. J., & El Hadi, H. (2005). The tectonic frame of the Variscan–Alleghanian orogen in Southern Europe and Northern Africa. *Tectonophysics*, *398*(3–4), 181–198. https://doi.org/10.1016/j.tecto.2005.02.006

Sláma, J., Košler, J., Condon, D. J., Crowley, J. L., Gerdes, A., Hanchar, J. M., et al. (2008). Plešovice zircon — A new natural reference material for U–Pb and Hf isotopic microanalysis. *Chemical Geology*, 249(1–2), 1–35. https://doi.org/10.1016/j.chemgeo.2007.11.005

Stern, R.S., Bodorkos S., Kamo S. L., Hickman, A. H., & Corfu F. (2009). Measurement of SIMS instrumental mass fractionation of Pb-isotopes during zircon dating. *Geostandards and Geoanalytical Research*, 33, pp. 145-168. https://doi.org/10.1111/j.1751-908X.2009.00023.x

Tahiri, A., & Hoepffner, C. (1988). Importance des mouvements distensifs au Dévonien supérieur en Meseta nord-occidentale (Maroc); les calcaires démantelés de Tiliouine et la ride d'Oulmès, prolongement oriental de la ride des Zaer. *Comptes Rendus de l'Académie Des Sciences de Paris*, *306*, 223–226.

Tahiri, A., Montero, P., El Hadi, H., Martínez Poyatos, D., Azor, A., Bea, F., et al. (2010). Geochronological data on the Rabat-Tiflet granitoids: their bearing on the tectonics of the Moroccan Variscides. *Journal of African Earth Sciences*, *57*(1–2), 1–13. https://doi.org/10.1016/j.jafrearsci.2009.07.005

Thirlwall, M. F., & Anczkiewicz, R. (2004). Multidynamic isotope ratio analysis using MC–ICP–MS and the causes of secular drift in Hf, Nd and Pb isotope ratios. *International Journal of Mass Spectrometry*, 235(1), 59–81.

https://doi.org/10.1016/j.ijms.2004.04.002

Tisserant, D. (1977). *Les isotopes du strontium et l'histoire hercynienne du Maroc. Etude de quelques massifs atlasiques et mésétiens.* Université Louis Pasteur, Strasbourg.

Van Hinsbergen, D. J. J., Torsvik, T. H., Schmid, S. M., Maţenco, L. C., Maffione, M., Vissers, R. L. M., et al. (2019). Orogenic architecture of the Mediterranean region and kinematic reconstruction of its tectonic evolution since the Triassic. *Gondwana Research*, *97*, 101145. https://doi.org/10.1016/j.gr.2019.07.009

Vermeesch, P. (2004). How many grains are needed for a provenance study? *Earth and Planetary Science Letters*, *224*(3–4), 441–451. https://doi.org/10.1016/j.epsl.2004.05.037

Vermeesch, P. (2012). On the visualisation of detrital age distributions. *Chemical Geology*, *312–313*, 190–194. https://doi.org/10.1016/j.chemgeo.2012.04.021

Vermeesch, P. (2018). Dissimilarity measures in detrital geochronology. *Earth-Science Reviews*, *178*(November 2017), 310–321. https://doi.org/10.1016/j.earscirev.2017.11.027

Villeneuve, M. (2008). Review of the orogenic belts on the western side of the West African craton: the Bassarides, Rokelides and Mauritanides. *Geological Society, London, Special Publications*, *297*(1), 169–201. https://doi.org/10.1144/SP297.8

Villeneuve, M., El Archi, A., & Nzamba, J. (2010). Les chaînes de la marge occidentale du Craton Ouest-Africain, modèles géodynamiques. *Comptes Rendus - Geoscience*, *342*(1), 1–10. https://doi.org/10.1016/j.crte.2009.12.002

Villeneuve, M., Gärtner, A., Youbi, N., El Archi, A., Vernhet, E., Rjimati, E.-C., et al. (2015). The southern and central parts of the "Souttoufide" belt, Northwest Africa. *Journal of African Earth Science*, *112*, 451–470. doi:10.1016/j.jafrearsci.2015.04.016

Wiedenbeck, M., Allé, P., Cordu, F., Griffin, W. L., Meier, M., Oberli, F., et al. (1995). Three natural zircon standards for U-Th-Pb, Lu-Hf, trace element and REE analyses. *Geostandards and Geoanalytical Research*, 19(1), 1–23. https://doi.org/10.1111/j.1751-908X.1995.tb00147.x

Woodhead, J., & Hergt, J. (2005). A Preliminary Appraisal of Seven Natural Zircon Reference Materials for In Situ Hf Isotope Determination. *Geostandards and Geoanalytical Research*, 29(2), 183–195. https://doi.org/10.1111/j.1751-908X.2005.tb00891.x

Woodhead, J., Hergt, J., Shelley, M., Eggins, S., & Kemp, R. (2004). Zircon Hf-isotope analysis with an excimer laser, depth profiling, ablation of complex geometries, and concomitant age estimation. *Chemical Geology*, 209(1–2), 121–135. https://doi.org/10.1016/j.chemgeo.2004.04.026

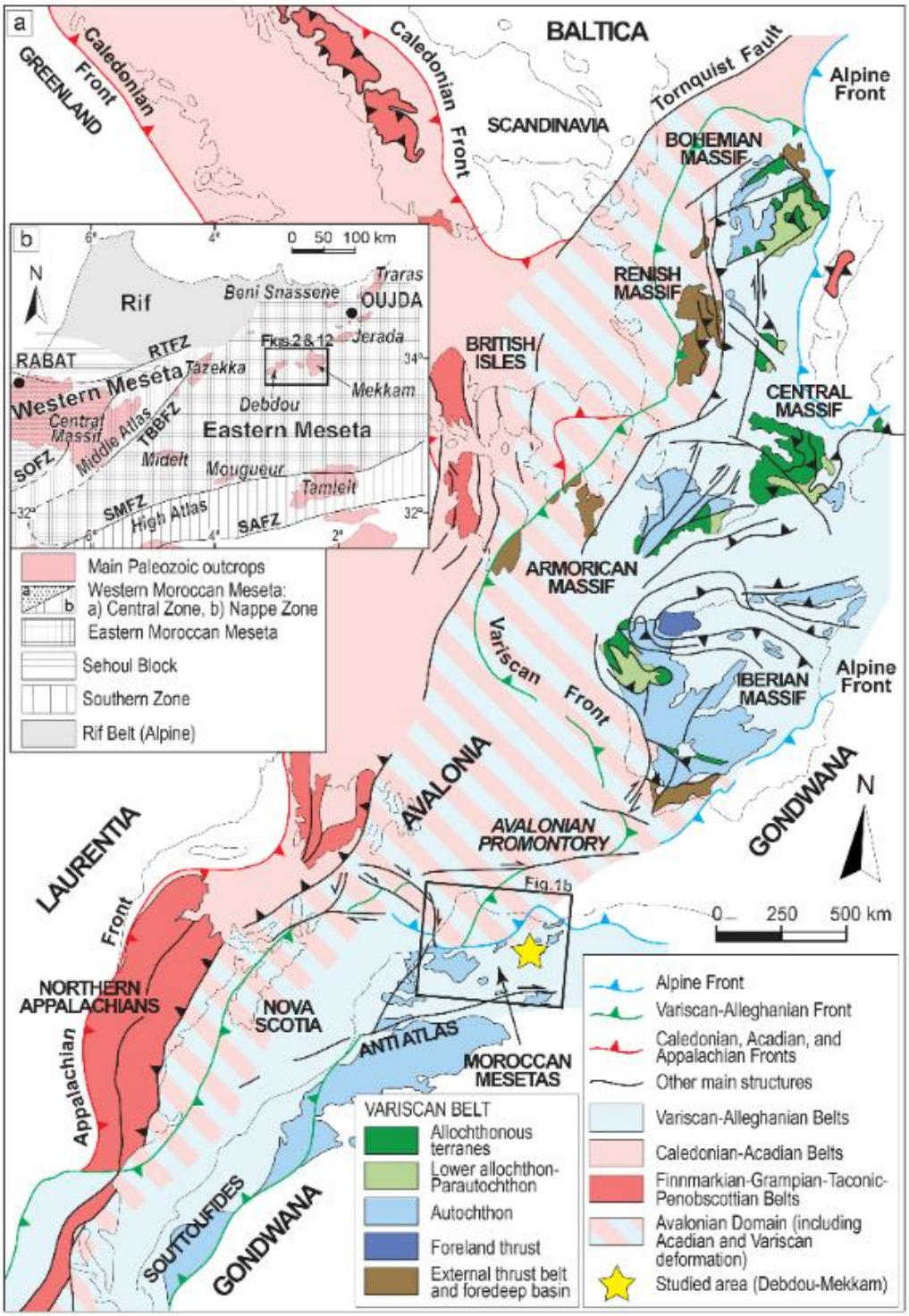

Figure 1: Large-scale geological setting of northern Morocco as part of the Variscan/Alleghanian Belt. (a) Reconstruction of the Variscan/Alleghanian and Caledonian belts at the end of the Paleozoic (modified from Martínez Catalán et al., 2002; Michard et al., 2010; Simancas et al., 2009). (b) Sketched geological map of the north-eastern Moroccan Variscides. RTFZ: Rabat-Tiflet Fault Zone; SOFZ: Smaala-Oulmès Fault Zone; TBBFZ: Tazekka-Bsabis-Bekrit Fault Zone; SMFZ: South Meseta Fault Zone; SAFZ: South Atlas Fault Zone (modified from Hoepffner et al., 2006; Michard et al., 2010).

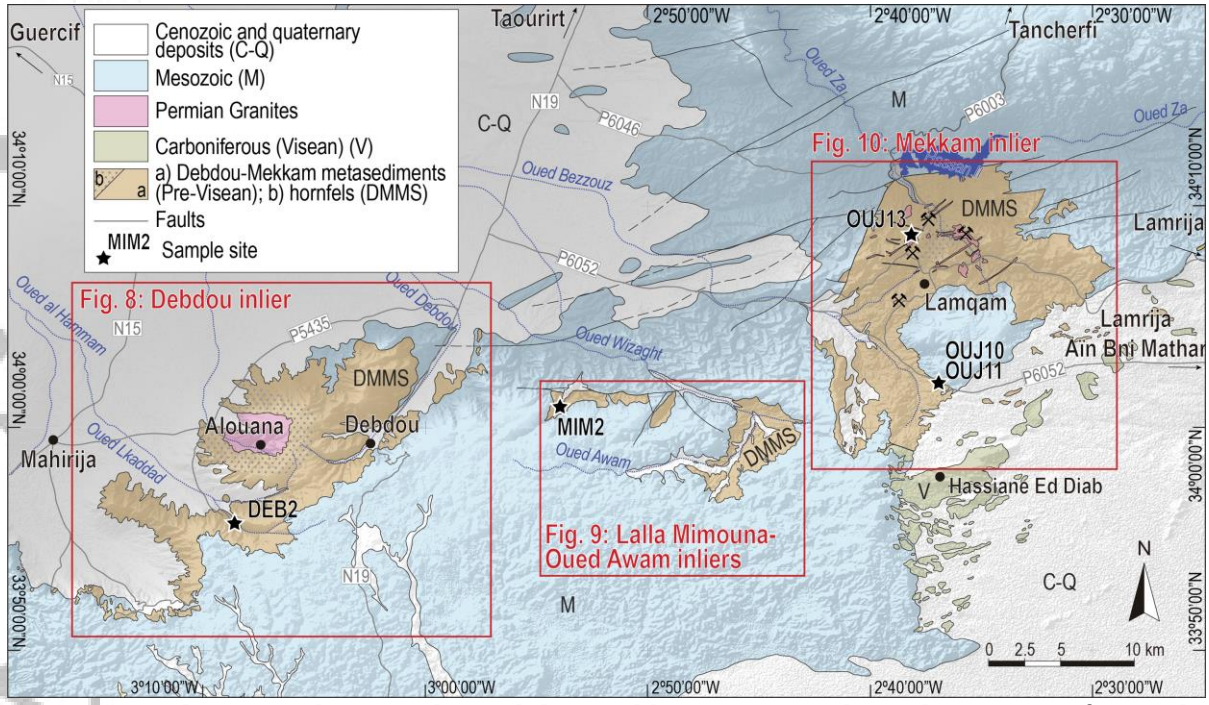

Figure 2. Paleozoic inliers in the Debdou-Mekkam region. The red squares refer to the detailed structural maps shown in Figures 8, 9, and 10. The topographic base is the Digital Earth Model SRTM 1 Arc-second Global (https://earthexplorer.usgs.gov/), with a superposed hillshade function to show altitude.

Figure 3. Main lithologies cropping out in the Debdou-Mekkam region: slates (a) and greywackes (b), which characterize the Debdou-Mekkam Metasediments (DMMS); cross-lamination in the slates (c) and graded bedding in a layer of greywackes (d) used as stratigraphic polarity criteria; (e) Upper Visean carbonate breccia with reworked clasts of DMMS slates (sl), volcanites (vl), and bioclasts (bc); (f) unconformity (U/C) between the previously deformed DMMS and the Visean succession (V) cropping out in the Hassian Ed Diab area: S0, stratigraphic bedding; S1, main cleavage.

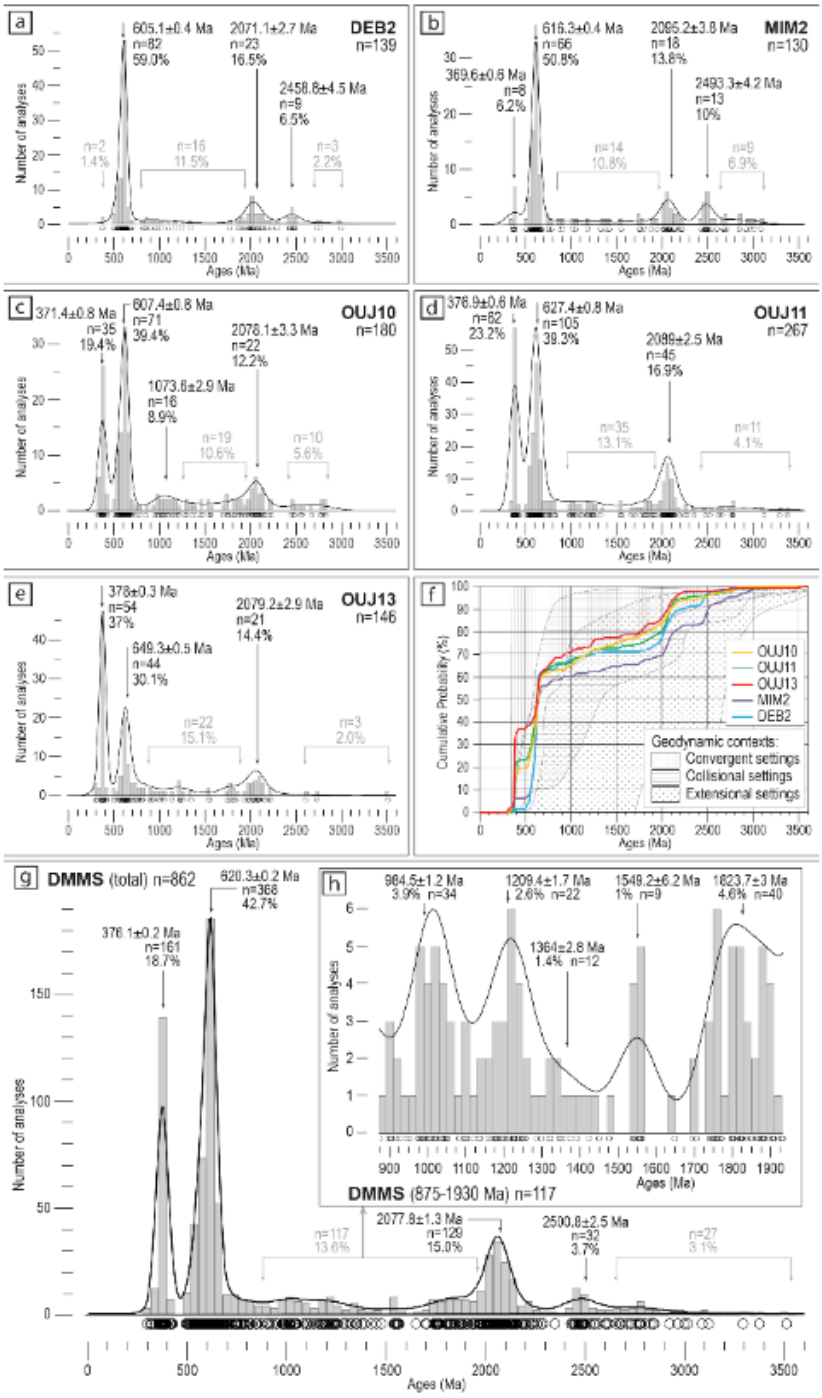

Figure 4. U-Pb results. (a-e) KDE (Kernel Density Estimator; black solid lines) and histogram (grey bars) plots showing the results of the detrital zircon U-Pb geochronological analyses for each sample; (f) Cumulative probability plot showing the results of the 5 samples from the DMMS and the cumulative areas typical of different geodynamic contexts (Cawood et al., 2012); (g) Cumulative KDE (black solid lines) and histogram (grey bars) for the DMMS and (h) zoom for the ages ranging from c. 900 to c. 1900 Ma. All the plots were built using $^{206}Pb/^{238}U$ ages for dates < 1500 Ma, $^{207}Pb/^{206}Pb$ ages for dates > 1500 Ma, and errors expressed at the 1σ level. KDE and histograms were performed with DensityPlotter 8.4 (Vermeesch, 2012).

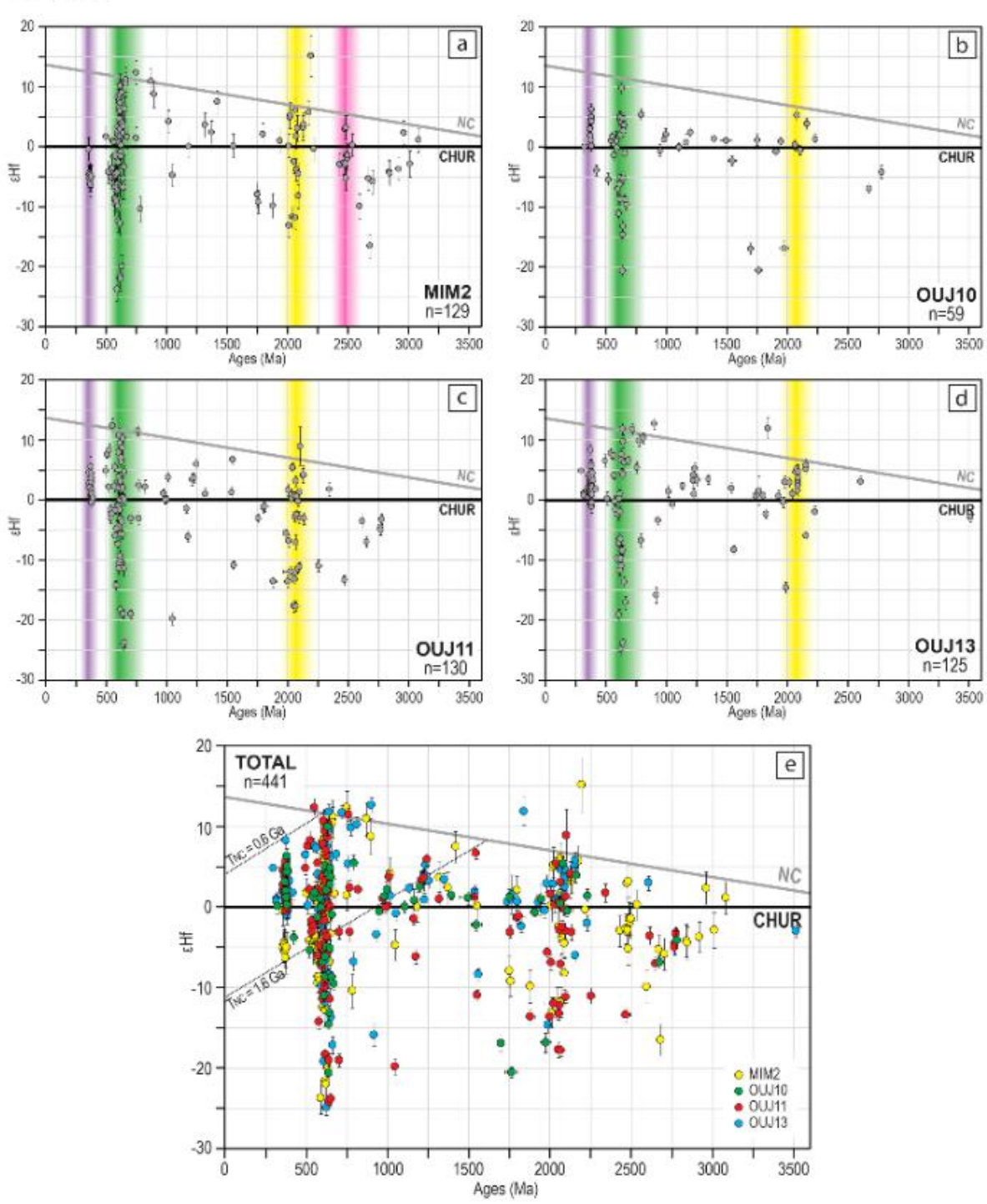

Figure 5. Mean ε_{Hf} values versus U-Pb ages plots for each sample (a-d) and cumulative (e). CHUR: Chondritic Uniform Reservoir (Bouvier et al., 2008); NC: new crust (Dhuime et al., 2011). The T_{NC} lines represent the bulk crust ($^{176}Lu/^{177}Hf$ = 0.015) corresponding with the new crust ages of the Devonian detrital zircon population. Colors bands indicate the main detrital zircon populations described in section 3.1: Late Devonian (purple), Ediacaran-Cryogenian (green), Paleoproterozoic (yellow), and Archean (pink).

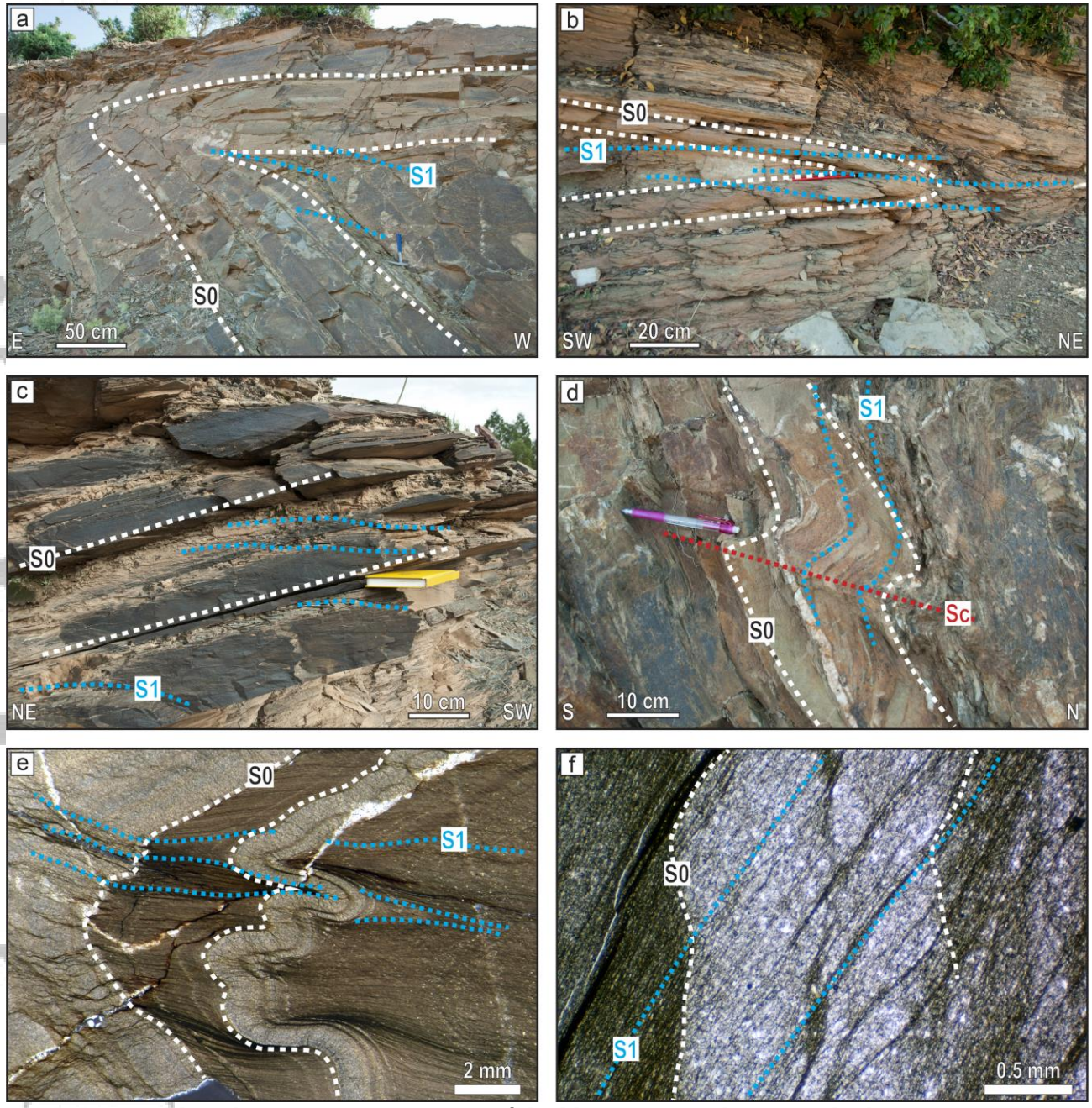

Figure 6. Field and microscopic images of bedding (S0) and principal cleavage (S1): mesoscale metric folds associated with S1 (a and b); S0/S1 relationships (c and d); microscale folds and axial plane cleavage, S1 (e); microscale relationships between S0 and S1 (f).

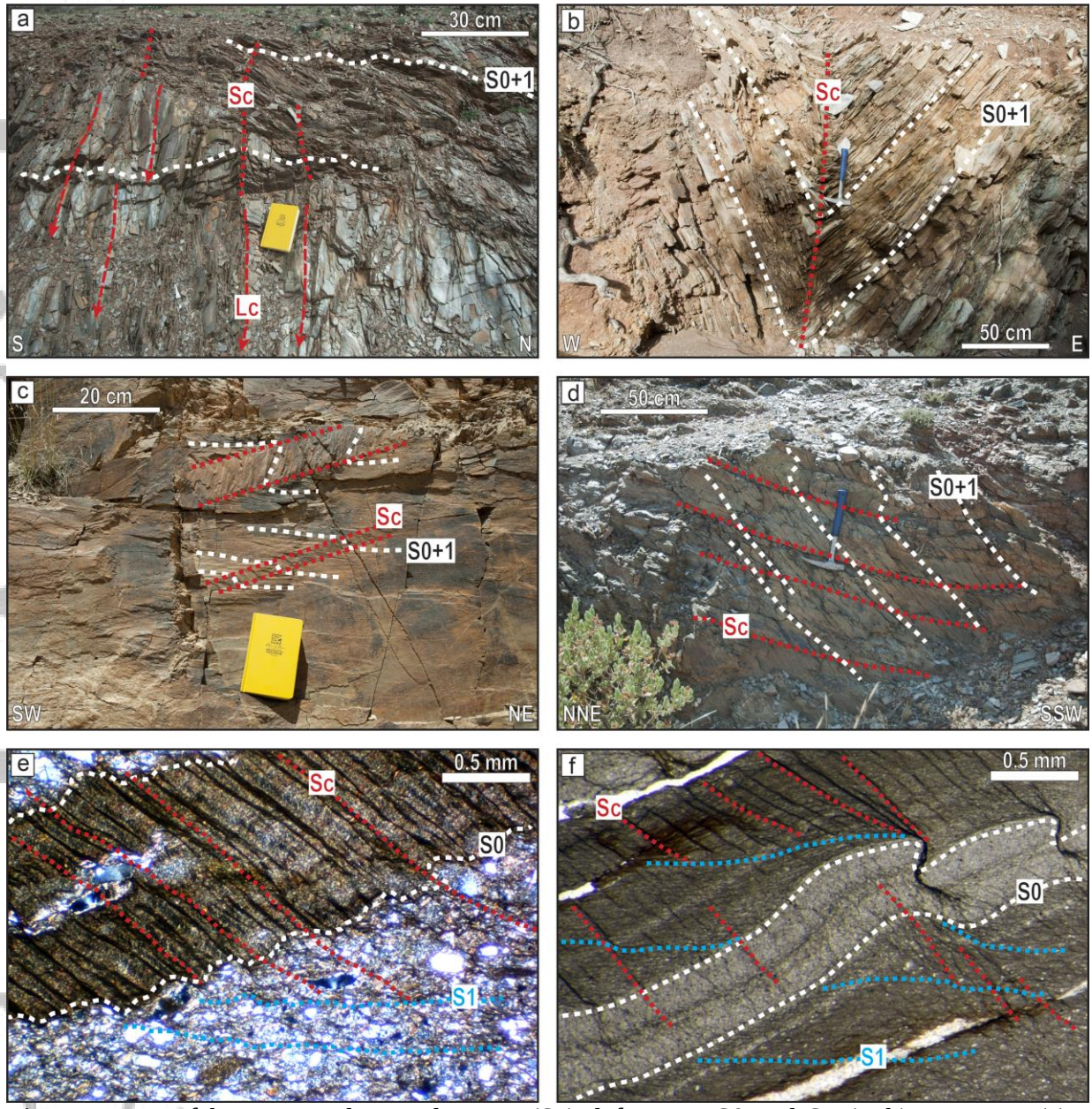

Figure 7. Late fabrics: crenulation cleavage (Sc) deforming S0 and S1 (a, b); incipient (c) and well developed (d) tectonic banding associated with a low-dipping crenulation cleavage; microscopic crenulation and its relationships with S0 and S1 (e, f).

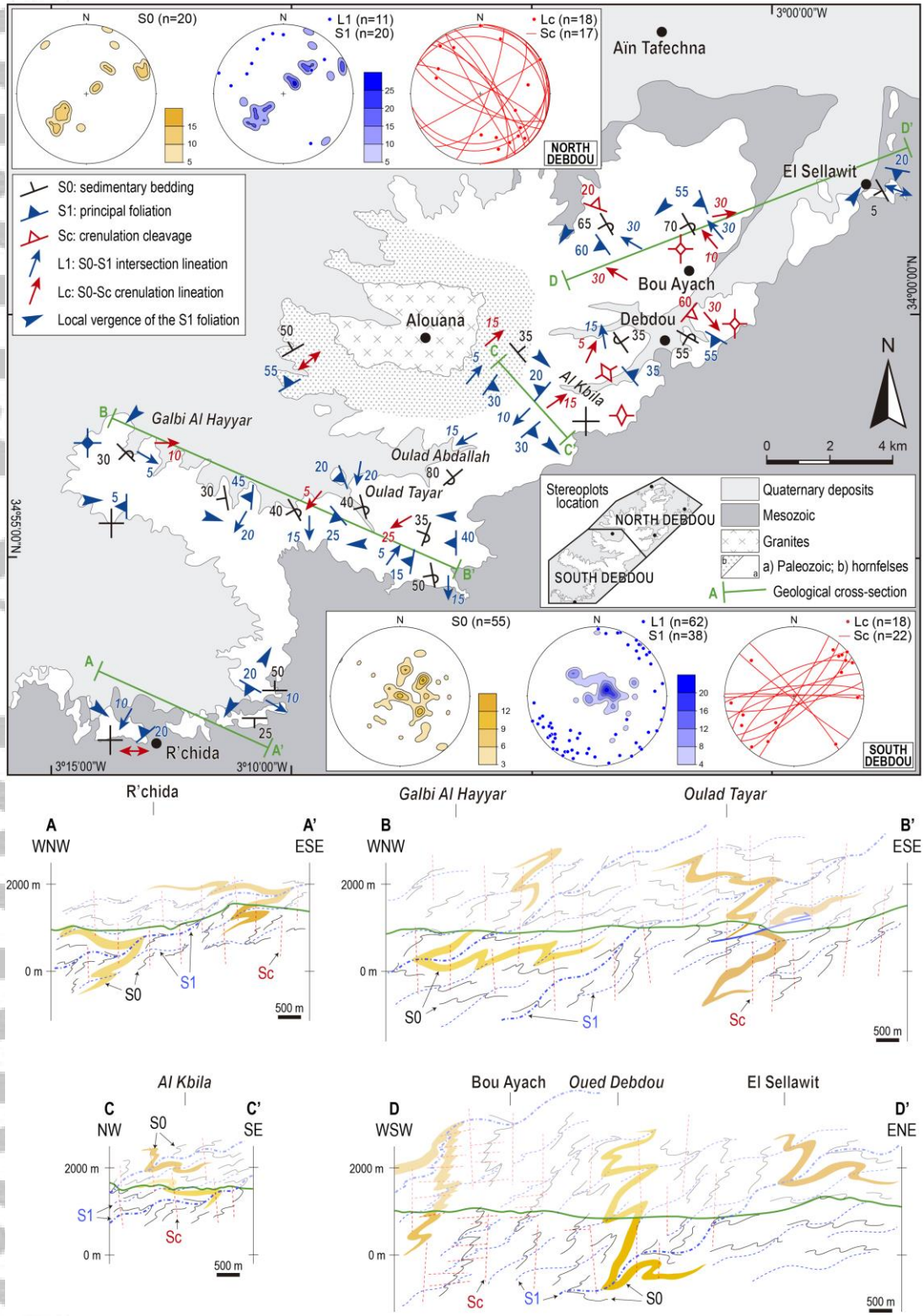

Figure 8 (previous page). Structural map and cross-sections of the Debdou inlier. Colors for different structural elements in the cross-sections correspond to those in the map.

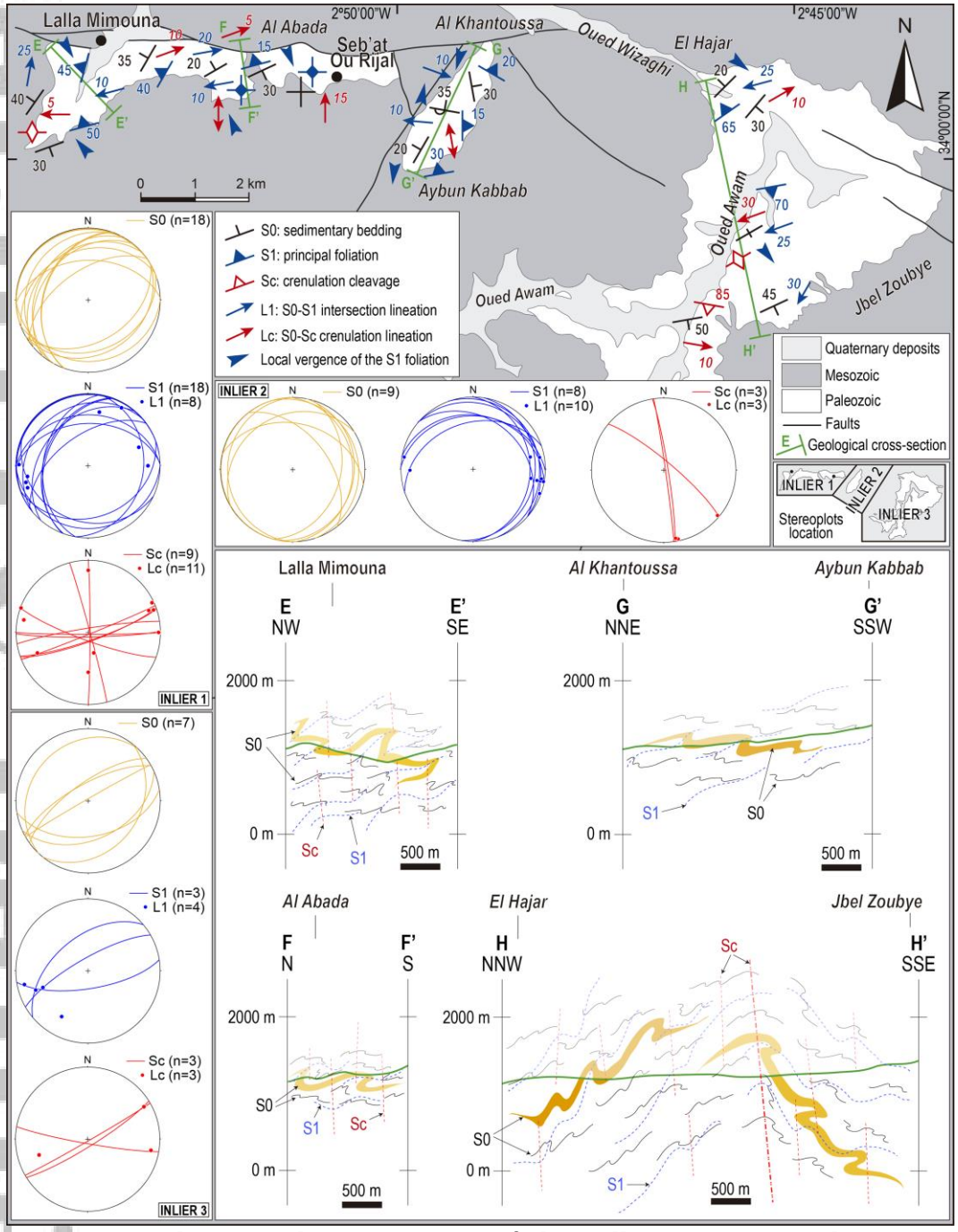

Figure 9. Structural map and cross-sections of the Lalla Mimouna-Oued Awam inliers. Colors for the different structural elements in the cross-sections correspond to those in the map.

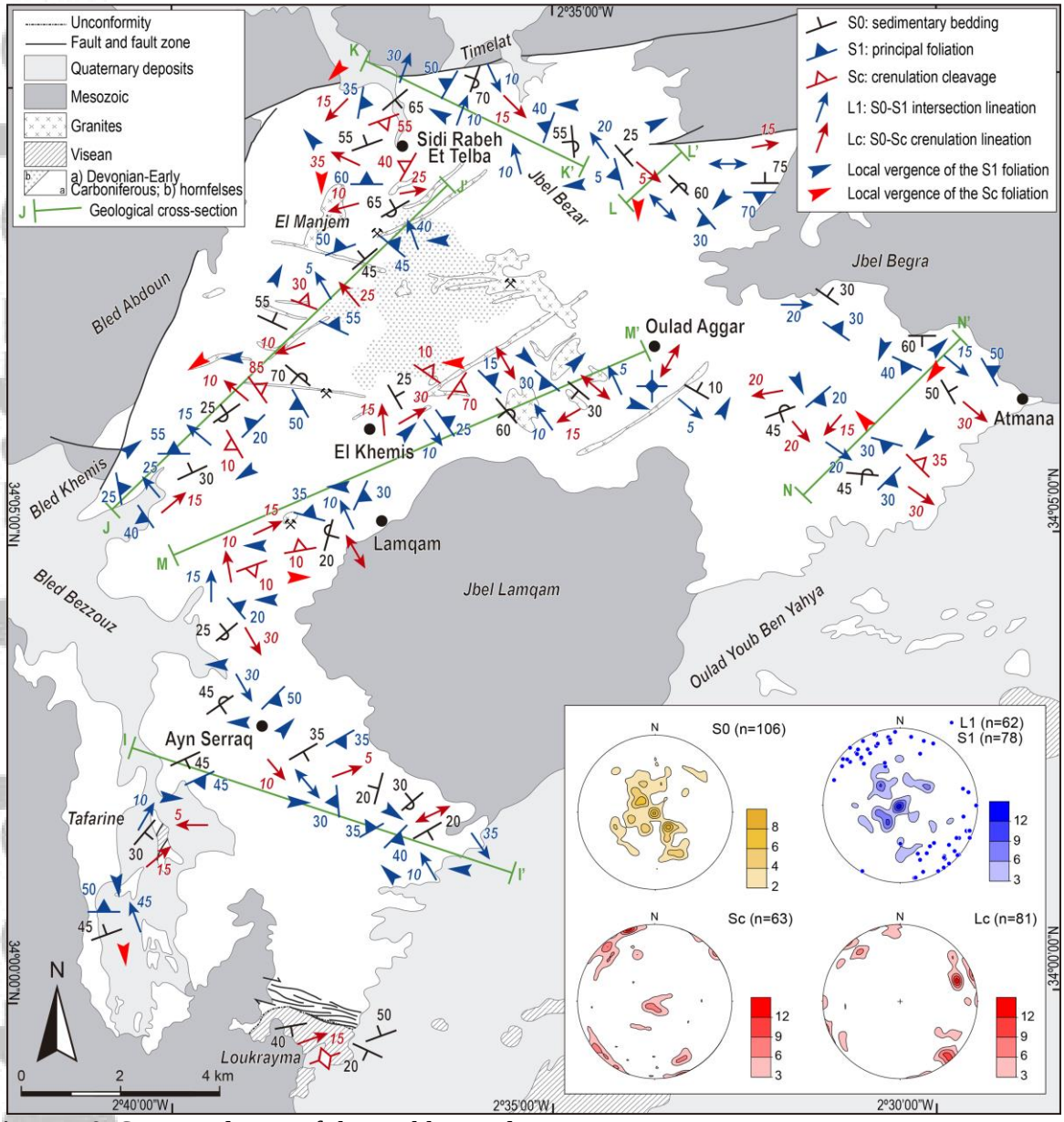

Figure 10. Structural map of the Mekkam inlier.

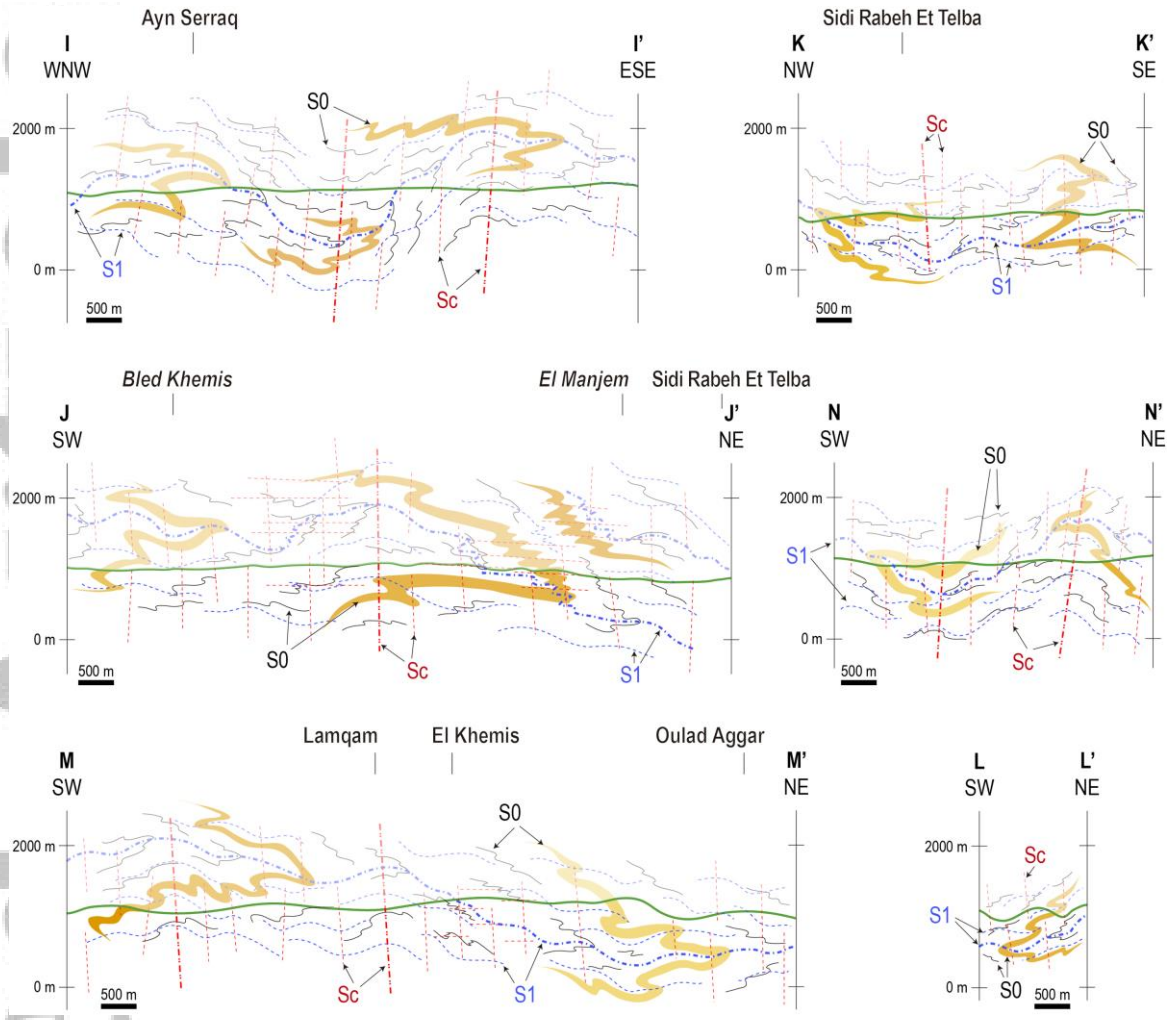

Figure 11. Cross-sections of the Mekkam inlier. See location in Figure 10. Colors of the different structural elements in the cross-sections correspond to those in the map.

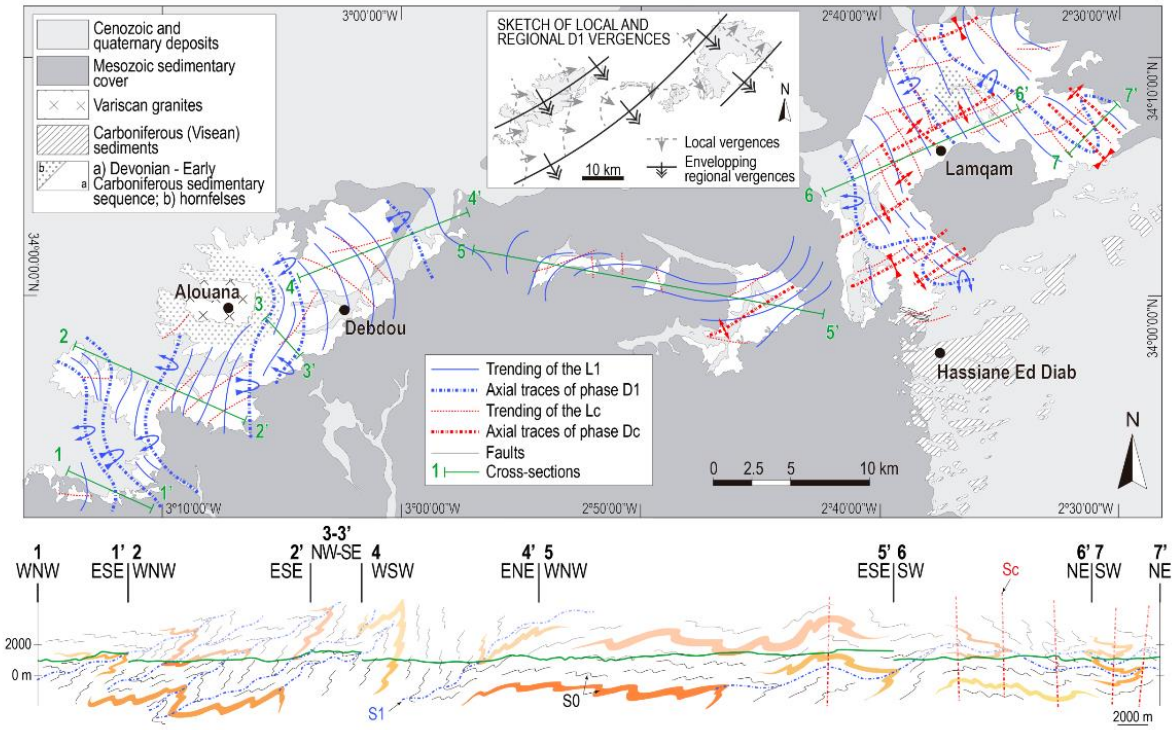

Figure 12. Synthetic map and cross-sections of the Debdou-Mekkam region. Colors of the different structural elements in the cross-sections correspond to those in the map. Inset: sketch of the local and regional vergences of the D1 structures. See Figure 1b for a more general geological sketch with the location of the inliers.

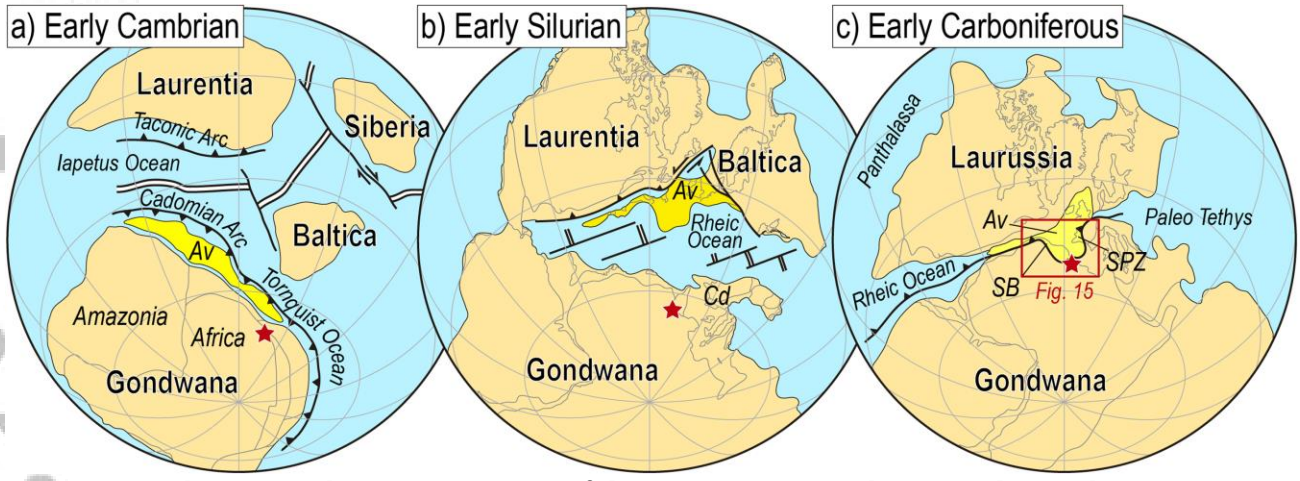

Figure 13. Paleogeographic reconstruction of the main continents during Early Cambrian (a), Early Silurian (b), and Early Carboniferous times (c). Av: Avalonia, Cd: Cadomia, SB: Sehoul Block, SPZ: South Portuguese Zone (after Murphy et al., 2016 and references therein; Nance et al., 2012 and references therein). Red stars indicate the approximate location of the studied area.

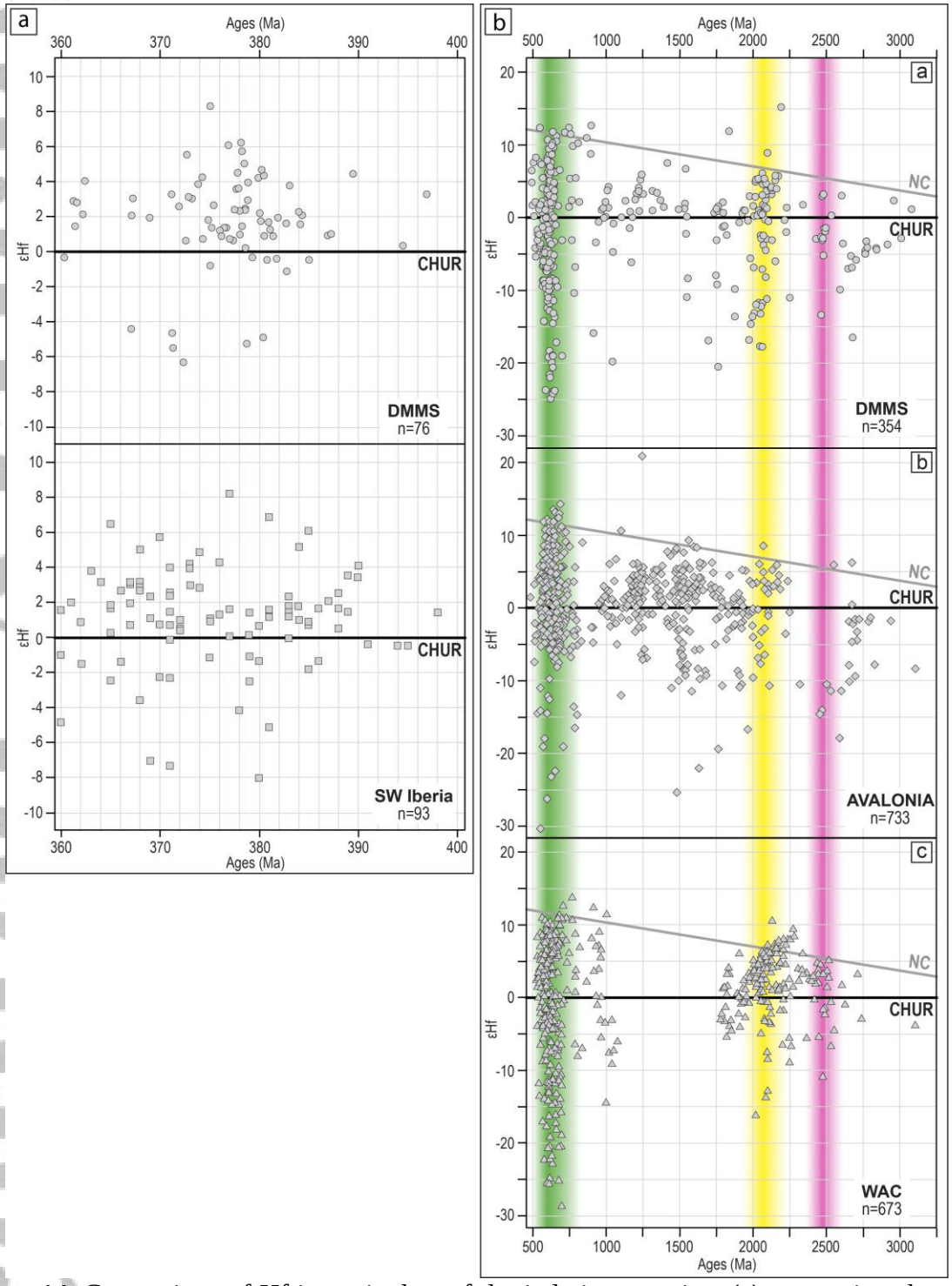

Figure 14. Comparison of Hf isotopic data of detrital zircon grains: (a) comparison between Devonian (400-360 Ma) data from DMMS (this work) and from SW Iberia (Pereira et al., 2017); (b) comparison among pre-Devonian (3250-450 Ma) data from DMMS (this work), Avalonian terranes (modified from Henderson et al., 2018 and references therein), and WAC (Abati et al., 2012; Avigad et al., 2012). Colors indicate some of the main detrital zircon populations identified in this work: Ediacaran-Cryogenian (green), Paleoproterozoic (yellow), and Archean (pink).

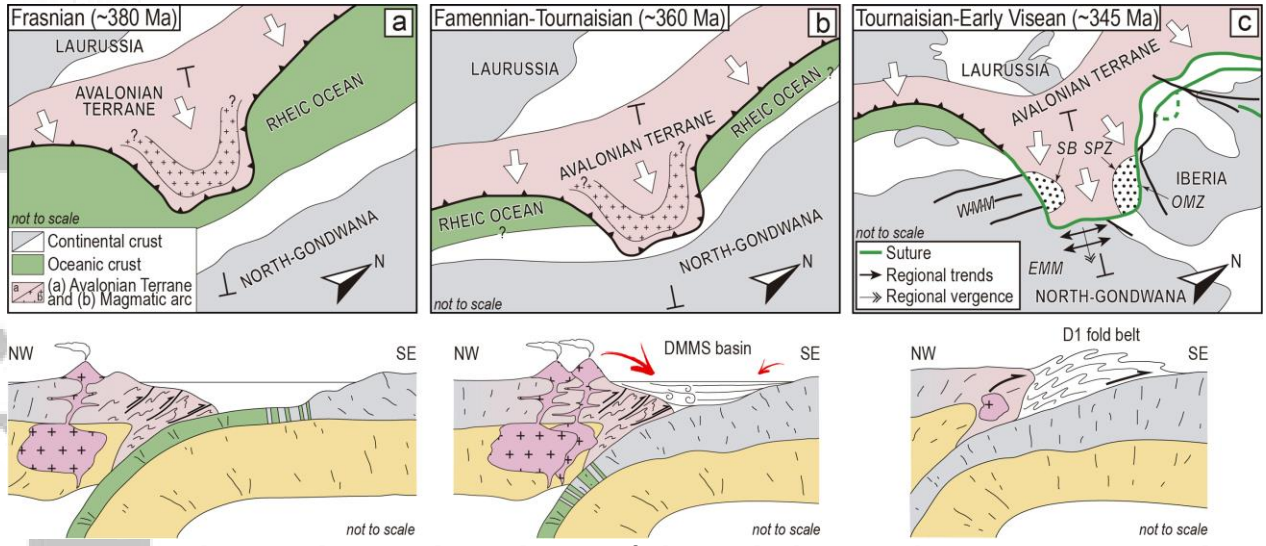

Figure 15. Schematic large-scale evolution of the studied region between Frasnian and Tournaisian time. SH: Sehoul Block; WMM: Western Moroccan Meseta; EMM: Eastern Moroccan Meseta; SPZ: South Portuguese Zone; OMZ: Ossa-Morena Zone (modified from Pereira et al. (2017) and Simancas et al. (2005)).